Geoscience Frontiers 11 (2020) 2083–2102

HOSTED BY

Contents lists available at ScienceDirect

Geoscience Frontiers

journal homepage: www.elsevier.com/locate/gsf

Research Paper

# Ophiolite hosted chromitite formed by supra-subduction zone peridotite –plume interaction

Júlia Farré-de-Pablo [a,*], Joaquín A. Proenza [a], José María González-Jiménez [b], Thomas Aiglsperger [c], Antonio Garcia-Casco [b,d], Javier Escuder-Viruete [e], Vanessa Colás [f], Francisco Longo [g]

[a] Departament de Mineralogia, Petrologia i Geologia Aplicada, Universitat de Barcelona, C/ Martí i Franquès, s/n, 08028, Barcelona, Spain
[b] Departamento de Mineraloga y Petrologa, Universidad de Granada, Facultad de Ciencias, Fuentenueva s/n, 18002, Granada, Spain
[c] Department of Civil Engineering and Natural Resources, Luleå University of Technology, SE 97187, Luleå, Sweden
[d] Instituto Andaluz de Ciencias de la Tierra (CSIC-UGR), Avda. de las Palmeras 4, E-18100, Armilla, Granada, Spain
[e] Instituto Geológico y Minero de España, C/ La Calera 1, Tres Cantos, 28760, Madrid, Spain
[f] Instituto de Geología, Universidad Nacional Autónoma de México, Ciudad Universitaria, 04510, Ciudad de México, Mexico
[g] Facultad de Ingeniería, Universidad Católica de Cibao, La Vega, Dominican Republic

ARTICLE INFO

Handling Editor: Kristoffer Szilas

*Keywords:*
Chromitite
Ophiolite
Plume
Mantle
Back-arc basin
Dominican Republic

ABSTRACT

Chromitite bodies hosted in peridotites typical of suboceanic mantle (*s.l.* ophiolitic) are found in the northern and central part of the Loma Caribe peridotite, in the Cordillera Central of the Dominican Republic. These chromitites are massive pods of small size (less than a few meters across) and veins that intrude both dunite and harzburgite. Compositionally, they are high-Cr chromitites [Cr# = Cr/(Cr + Al) atomic ratio = 0.71–0.83] singularly enriched in $TiO_2$ (up to 1.25 wt.%), $Fe_2O_3$ (2.77–9.16 wt.%) as well as some trace elements (Ga, V, Co, Mn, and Zn) and PGE (up to 4548 ppb in whole-rock). This geochemical signature is unknown for chromitites hosted in oceanic upper mantle but akin to those chromites crystallized from mantle plume derived melts. Noteworthy, the melt estimated to be in equilibrium with such chromite from the Loma Caribe chromitites is similar to basalts derived from different source regions of a heterogeneous Caribbean mantle plume. This mantle plume is responsible for the formation of the Caribbean Large Igneous Province (CLIP). Dolerite dykes with back-arc basin basalt (BABB) and enriched mid-ocean ridge basalt (E-MORB) affinities commonly intrude the Loma Caribe peridotite, and are interpreted as evidence of the impact that the Caribbean plume had in the off-axis magmatism of the back-arc basin, developed after the Caribbean island-arc extension in the Late Cretaceous. We propose a model in which chromitites were formed in the shallow portion of the back-arc mantle as a result of the metasomatic reaction between the supra-subduction zone (SSZ) peridotites and upwelling plume-related melts.

## 1. Introduction

Chromitites mainly consist of (Cr, Al)-rich spinel and are usually found associated with mafic-ultramafic rocks, such as in layered intrusions (e.g., Mukherjee et al., 2010), anorthositic complexes (e.g., Rollinson et al., 2010), Ural-Alaskan type complexes (e.g., Garuti et al., 2003) and the mantle section of ophiolites (e.g., Barnes and Roeder, 2001; O'Driscoll and González-Jiménez, 2016; Mathez and Kinzler, 2017). The latter exhibit a wide range of morphologies (e.g., pods, vein, bands, etc.) and are frequently hosted within dunites formed by metasomatic reaction between migrating basaltic melts and depleted peridotites within mid-ocean ridge or, more commonly, supra-subduction zone (SSZ) settings (González-Jiménez et al., 2014b; Arai and Miura, 2016). These types of chromitites are collectively grouped as ophiolitic, and their formation has been traditionally associated with the infiltration of basaltic melts reaching the mantle-crust transition zone of the oceanic lithosphere (e.g., Arai and Yurimoto, 1994; Zhou et al., 1994; Melcher et al., 1997; Proenza et al., 1999; Gervilla et al., 2005). From a compositional point of view, ophiolitic chromitites are classified as high-Cr [Cr# = Cr/(Cr + Al), atomic ratio

* Corresponding author.
*E-mail address:* jfarredepablo@gmail.com (J. Farré-de-Pablo).
Peer-review under responsibility of China University of Geosciences (Beijing).

https://doi.org/10.1016/j.gsf.2020.05.005
Received 22 January 2020; Received in revised form 17 March 2020; Accepted 6 May 2020
Available online 19 May 2020

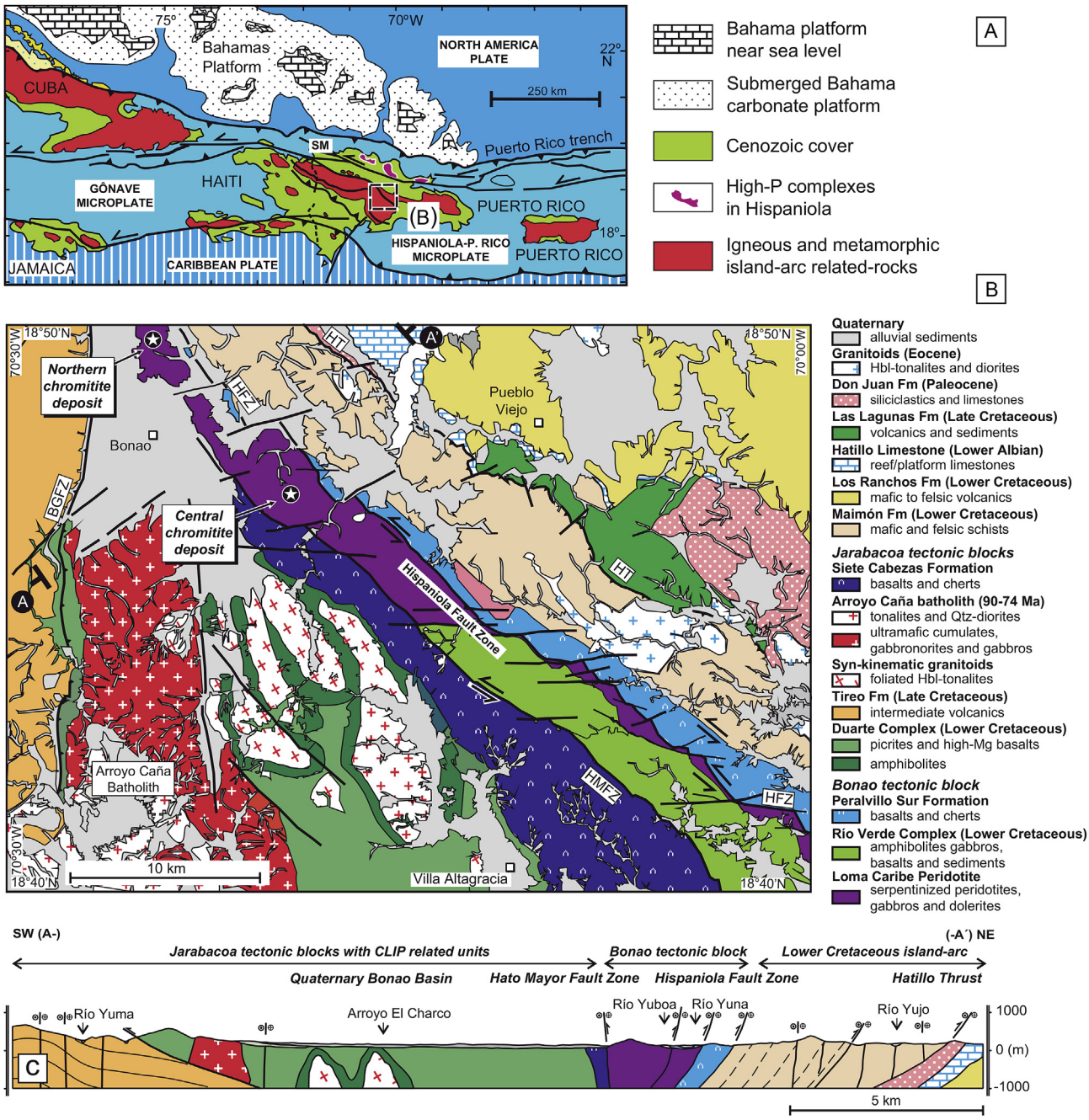


**Fig. 1.** (A) Map of the northeastern Caribbean plate margin. Box shows location of the study area. SM, Septentrional microplate. (B) Schematic geological map of the Bonao 1:100,000 quadrangle and (C) A–A′ geological cross-section (modified from Gómez et al., 1999), showing the lithologic and structural relations between the Jarabacoa tectonic block with the Caribbean Large Igneous Province (CLIP) units, Bonao tectonic block including the Loma Caribe peridotite, and the Lower Cretaceous island-arc units (modified from Escuder-Viruete et al., 2007, 2009). HFZ, Hispaniola fault zone; HMFZ, Hato Mayor fault zone; and HT, Hatillo thrust. Stars show locations of chromitite samples.

>0.6] and high-Al (Cr# <0.6). High-Cr chromitites are usually depleted in $TiO_2$ (<0.25 wt.%; Leblanc and Nicolas, 1992) and enriched in PGE relative to high-Al chromitites, which are typically enriched in $TiO_2$ (~0.5 wt.%) but depleted in PGE (e.g., González-Jiménez et al., 2011; González-Jiménez et al., 2014b). Typically, high-Cr chromitites exhibit a geochemical signature similar to that of boninitic lavas, being interpreted as having formed in fore-arc regions in supra-subduction zones (SSZ) when subduction initiates. In contrast, high-Al chromitites precipitate from basaltic melts with mid-ocean ridge basalt (MORB) affinity, indicating abyssal or back-arc settings of formation. Hence, ophiolitic chromitites are thought to have formed in different geodynamic settings within the ophiolite environment (Zhou et al., 1994, 1998; Robinson et al., 1997; Ballhaus, 1998; Ahmed and Arai, 2002; Miura et al., 2012).

More recent models, based on the discovery of an unprecedented suite of minerals typically formed at ultra-high pressures (e.g., diamond, coesite, $TiO_2$-II; i.e., the UHP assemblage of Yamamoto et al., 2009), and super-reducing conditions (e.g., native elements, alloys, carbides, nitrides, moissanite; i.e., the SuR assemblage of Griffin et al., 2016 and Pujol-Solà et al., 2018), and crustal minerals (e.g., zircon, K-feldspar, plagioclase, kyanite, garnet, quartz; Robinson et al., 2015), reveal a more complex evolutionary history of chromitites associated with the oceanic mantle. Some of the proposed models include (e.g., Rollinson, 2016): (1) *subduction-recycling* (Arai, 2013; McGowan et al., 2015; Arai and Miura,

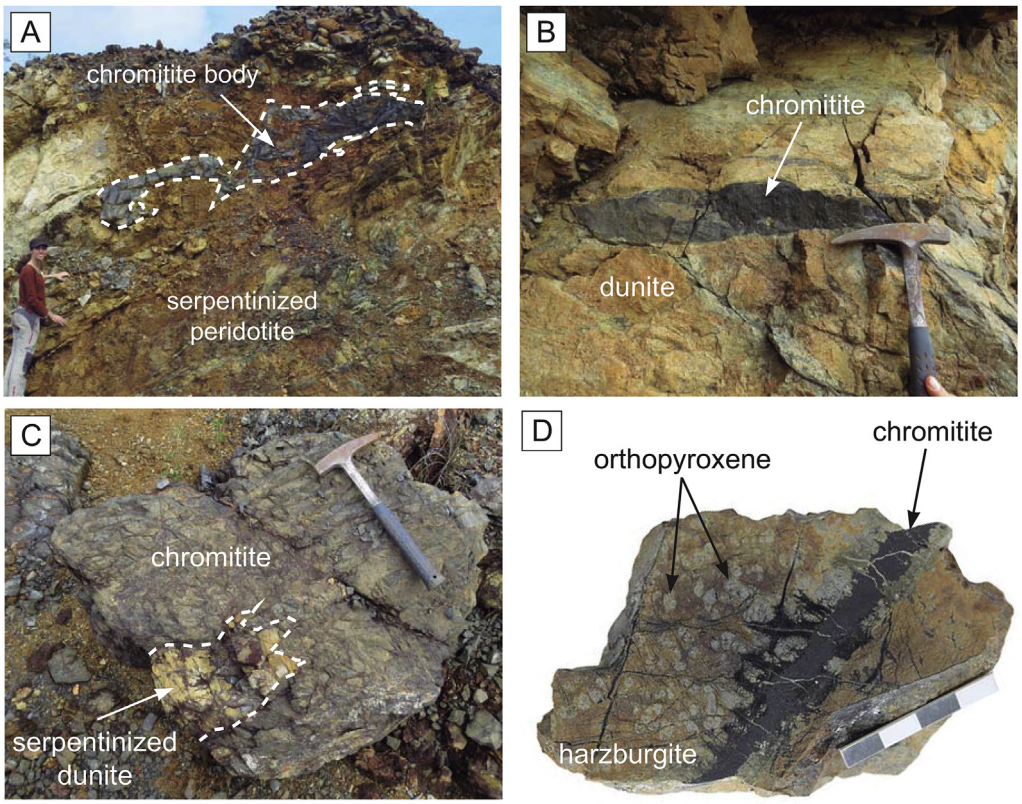


**Fig. 2.** (A–C) Field photographs of the outcrops showing morphologies and structures of the studied chromitite deposits. (D) Hand sample of a chromitite vein hosted in harzburgite. The scale bar is 4 cm.

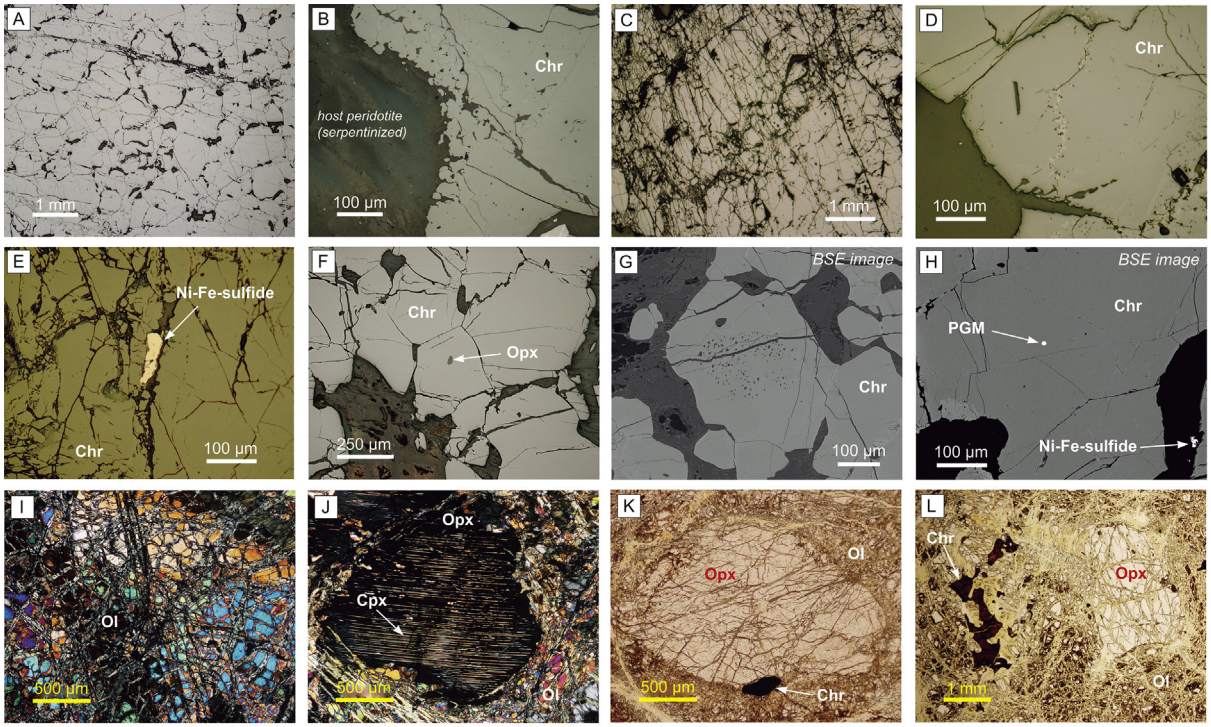


**Fig. 3.** Textural details of the studied chromitites (A–H) and host peridotite (I–L). (A) Unaltered massive chromitites with interstitial altered silicates (reflected light). (B) Contact of massive chromitite with serpentinized host peridotite (reflected light). (C) Penetrative fractures affecting massive chromitites (reflected light). (D) Slight chemical variations along fractures in chromite grains (reflected light). (E) Ni–Fe-sulfides within fractures across chromitites (reflected light). (F) Mineral inclusions of primary silicates within chromite grains (reflected light). (G) Silicate inclusions clustered within chromite grain (backscattered electron image). (H) PGM inclusion within chromite grain (backscattered electron image). (I) Olivine grains with undulose extinction cross-cut by serpentine veins (transmitted light). (J) Orthopyroxene grain with clinopyroxene lamellae along cleavage and olivine surrounding the grain (transmitted light). (K) Subhedral accessory chromite next to orthopyroxene grain (transmitted light). (L) Vermicular accessory chromite associated with orthopyroxene, olivine and minor clinopyroxene. Chr = chromite; Opx = orthopyroxene; PGM = platinum group mineral; Cpx = clinopyroxene; Ol = olivine.

**Table 1**
Representative results of electron-microprobe analyses of chromite from the studied chromitites. Complete data set can be found in Appendix B.

| | Massive pods | Massive pods | Massive pods | Massive pods | Massive pods | Massive pods | Massive pods | Massive pods | Massive pods | Massive pods | Massive pods | Massive pods | Massive pods | Massive pods | Massive pods |
|---|---|---|---|---|---|---|---|---|---|---|---|---|---|---|---|
| | LC-chromitite-3-0 | LC-chromitite-3-4 | LC-chromitite-3-9 | LC-chromitite-3-11 | LC-chromitite-3-18 | LC-chromitite-3-21 | LC-chromitite-3-32 | LC-chromitite-3-36 | LC-chromitite-3-48 | LC-17-1-p3-3 | LC-17-1-p4-1 | LC-17-1-p5-2 | LC-17-1-p8-1 | LC-17-1-p8-3 | LP1-95-91 |
| wt.% | | | | | | | | | | | | | | | |
| $SiO_2$ | b.d.l. | b.d.l. | 0.02 | 0.02 | b.d.l. | b.d.l. | b.d.l. | b.d.l. | 0.02 | b.d.l. | b.d.l. | b.d.l. | b.d.l. | b.d.l. | 0.14 |
| $TiO_2$ | 0.65 | 0.49 | 0.70 | 0.59 | 0.43 | 0.62 | 0.56 | 0.70 | 0.82 | 0.39 | 0.41 | 0.43 | 0.42 | 0.29 | 0.88 |
| $Al_2O_3$ | 11.67 | 11.47 | 11.30 | 11.57 | 11.64 | 11.90 | 11.78 | 11.84 | 11.65 | 10.76 | 10.41 | 10.97 | 10.92 | 8.40 | 9.96 |
| $Cr_2O_3$ | 55.64 | 55.84 | 55.67 | 56.34 | 56.14 | 55.61 | 55.34 | 55.46 | 55.60 | 57.77 | 58.05 | 57.19 | 57.38 | 60.24 | 52.89 |
| FeO | 14.80 | 15.02 | 16.05 | 14.91 | 14.77 | 14.77 | 14.66 | 14.94 | 15.02 | 16.30 | 16.28 | 16.47 | 16.26 | 17.06 | 19.97 |
| $Fe_2O_3$ | 4.06 | 4.28 | 3.75 | 3.77 | 4.01 | 3.87 | 4.18 | 4.01 | 3.82 | 2.90 | 2.97 | 3.15 | 3.44 | 2.77 | 7.02 |
| MnO | 0.31 | 0.31 | 0.33 | 0.26 | 0.30 | 0.32 | 0.30 | 0.32 | 0.30 | 0.14 | 0.12 | 0.12 | 0.16 | 0.16 | 0.32 |
| MgO | 12.47 | 12.22 | 11.60 | 12.49 | 12.37 | 12.48 | 12.46 | 12.45 | 12.46 | 11.28 | 11.28 | 11.24 | 11.40 | 10.44 | 9.09 |
| NiO | 0.18 | 0.18 | 0.20 | 0.19 | 0.20 | 0.23 | 0.18 | 0.21 | 0.21 | 0.25 | 0.26 | 0.25 | 0.26 | 0.20 | 0.21 |
| ZnO | 0.13 | 0.14 | 0.10 | 0.08 | 0.12 | 0.11 | 0.15 | 0.12 | 0.10 | 0.12 | 0.12 | 0.11 | 0.13 | 0.14 | 0.21 |
| Total | 99.92 | 99.94 | 99.73 | 100.22 | 99.99 | 99.92 | 99.62 | 100.03 | 99.98 | 99.91 | 99.90 | 99.94 | 100.37 | 99.71 | 100.69 |
| apfu | | | | | | | | | | | | | | | |
| Si | b.d.l. | b.d.l. | 0.00 | 0.00 | b.d.l. | b.d.l. | b.d.l. | b.d.l. | 0.00 | b.d.l. | b.d.l. | b.d.l. | b.d.l. | b.d.l. | 0.00 |
| Ti | 0.02 | 0.01 | 0.02 | 0.01 | 0.01 | 0.02 | 0.01 | 0.02 | 0.02 | 0.01 | 0.01 | 0.01 | 0.01 | 0.01 | 0.02 |
| Al | 0.44 | 0.44 | 0.43 | 0.44 | 0.44 | 0.45 | 0.45 | 0.45 | 0.44 | 0.42 | 0.40 | 0.42 | 0.42 | 0.33 | 0.39 |
| Cr | 1.42 | 1.43 | 1.44 | 1.44 | 1.43 | 1.42 | 1.42 | 1.41 | 1.42 | 1.49 | 1.50 | 1.48 | 1.48 | 1.59 | 1.39 |
| $Fe^{2+}$ | 0.40 | 0.41 | 0.44 | 0.40 | 0.40 | 0.40 | 0.40 | 0.40 | 0.41 | 0.45 | 0.45 | 0.45 | 0.44 | 0.48 | 0.55 |
| $Fe^{3+}$ | 0.10 | 0.10 | 0.09 | 0.09 | 0.10 | 0.09 | 0.10 | 0.10 | 0.09 | 0.07 | 0.07 | 0.08 | 0.08 | 0.07 | 0.18 |
| Mn | 0.01 | 0.01 | 0.01 | 0.01 | 0.01 | 0.01 | 0.01 | 0.01 | 0.01 | 0.00 | 0.00 | 0.00 | 0.00 | 0.00 | 0.01 |
| Mg | 0.60 | 0.59 | 0.56 | 0.60 | 0.60 | 0.60 | 0.60 | 0.60 | 0.60 | 0.55 | 0.55 | 0.55 | 0.55 | 0.52 | 0.45 |
| Ni | 0.00 | 0.00 | 0.01 | 0.00 | 0.01 | 0.01 | 0.00 | 0.01 | 0.01 | 0.01 | 0.01 | 0.01 | 0.01 | 0.01 | 0.01 |
| Zn | 0.00 | 0.00 | 0.00 | 0.00 | 0.00 | 0.00 | 0.00 | 0.00 | 0.00 | 0.00 | 0.00 | 0.00 | 0.00 | 0.00 | 0.01 |
| Cr# | 0.76 | 0.77 | 0.77 | 0.77 | 0.76 | 0.76 | 0.76 | 0.76 | 0.76 | 0.78 | 0.79 | 0.78 | 0.78 | 0.83 | 0.78 |
| Mg# | 0.60 | 0.59 | 0.56 | 0.60 | 0.60 | 0.60 | 0.60 | 0.60 | 0.60 | 0.55 | 0.55 | 0.55 | 0.56 | 0.52 | 0.45 |
| $Fe^{3+}$# | 0.10 | 0.11 | 0.10 | 0.10 | 0.10 | 0.10 | 0.11 | 0.10 | 0.10 | 0.08 | 0.08 | 0.08 | 0.09 | 0.08 | 0.16 |
| FeO/$Fe_2O_3$ | 3.64 | 3.51 | 4.28 | 3.96 | 3.68 | 3.81 | 3.51 | 3.73 | 3.93 | 5.63 | 5.47 | 5.23 | 4.73 | 6.17 | 2.84 |
| *Estimated composition for parental melts* | | | | | | | | | | | | | | | |
| $Al_2O_3$ (wt.%) | 11.72 | 11.63 | 11.55 | 11.67 | 11.70 | 11.82 | 11.76 | 11.79 | 11.71 | 11.29 | 11.12 | 11.39 | 11.37 | 10.00 | 10.89 |
| $TiO_2$ (wt.%) | 0.80 | 0.62 | 0.85 | 0.73 | 0.55 | 0.77 | 0.69 | 0.85 | 0.98 | 0.51 | 0.54 | 0.56 | 0.54 | 0.40 | 1.05 |
| FeO/MgO | 0.92 | 0.94 | 1.06 | 0.92 | 0.92 | 0.92 | 0.91 | 0.93 | 0.93 | 1.10 | 1.09 | 1.12 | 1.09 | 1.19 | 1.61 |

Cations calculated on the basis of 32 oxygens; b.d.l. = below detection limit.

2016; Griffin et al., 2016), (2) *mantle plume model* (Ruskov et al., 2010; Xiong et al., 2015; Xu et al., 2015; Yang et al., 2015; Wu et al., 2016), and (3) *slab contamination* (Zhou et al., 2014; Robinson et al., 2015). These models have been recently challenged by Ballhaus et al. (2017), whose experimental results indicate that some of the nominally UHP and SuR minerals, including (micro)-diamonds, can be formed by quick condensation of high-T plasma originated by *lightning strikes* on chromitite bodies already exposed on the Earth's surface. However, natural evidence does not support a generalized formation of these minerals after lightning strikes (Farré-de-Pablo et al., 2018; Griffin et al., 2018; Pujol-Solà et al., 2018). All these models highlight that, in spite of decades of effort, the formation of chromitites in the oceanic mantle, as well as the suite of complex mineral assemblages that they usually enclose, is still unclear and hotly debated.

In this work, we contribute to this debate on the origin of ophiolitic chromitites with a suite of chromitite bodies hosted in mantle peridotites from the Loma Caribe peridotite, a section of oceanic mantle exhumed on-land in the Dominican Republic that is part of the large ophiolitic belt of the Greater Antilles (Lewis et al., 2006). The peridotites exhibit an intricacy of petrological and geochemical fingerprints resulting from a protracted multi-stage evolutionary history. This includes an initial stage of formation in a mid-ocean spreading-ridge environment and later modification during the opening and evolution of fore-arc and back-arc basins originated in an intra-oceanic arc (i.e., the Greater Antilles paleoarc; Lewis et al., 2006; Escuder-Viruete et al., 2008; Marchesi et al., 2016). In addition, the Loma Caribe peridotite was influenced by the magmatic activity related to the Caribbean mantle plume (Escuder-Viruete et al., 2008), which also produced the Caribbean Large Igneous Province (CLIP; Kerr et al., 1997). Proenza et al. (2007) reported an ophiolitic chromitite body from the central part of the Loma Caribe peridotite with anomalous Cr- and Ti-rich compositions, which they suggested to be possibly related to plume activity in the related upper oceanic mantle, although it was not positively confirmed. In this paper, we provide new data from the central chromitite body together with data from newly found chromitites in the northern part of the Loma Caribe peridotitic belt. We report new major and trace element analyses of chromite, and PGE geochemistry and mineralogy of the chromitites, and integrate these results with recent regional paleotectonic models of the northern Caribbean region to offer an explanation for the formation of these chromitites.

## 2. Geological background

The Dominican Republic in Hispaniola Island is part of the Great Arc of the Caribbean developed during the Cretaceous–Tertiary at the leading edge of the Caribbean Plate (Fig. 1). The island is a tectonic collage produced by the oblique convergence to final collision of the Caribbean island-arc/back-arc system with the North American continental margin (Mann et al., 1991; Draper et al., 1994; Pindell and Kennan, 2009). The presence of high-P mélanges and ophiolites in northern Hispaniola indicates that a proto-Caribbean oceanic basin was consumed by SW-directed subduction during the Early Cretaceous (Draper and Nagle, 1991; Krebs et al., 2008, 2011; Escuder-Viruete et al., 2011a, 2011c, 2014). Plutonic and volcanic rocks whose ages range from the Aptian to the lower Eocene record the magmatic activity in the Caribbean upper plate (Lewis and Draper, 1990; Kesler et al., 2005; Escuder-Viruete et al., 2006, 2008; Marchesi et al., 2016; Torró et al., 2017). A cover of Eocene to Holocene sedimentary rocks (Mann et al., 1991; Pérez-Estaún et al., 2007) regionally overlies the arc-related rocks and records the oblique arc-continent collision in northern Hispaniola, as well as the intra- and back-arc deformation (Mann et al., 2002; Escuder-Viruete et al., 2016).

Central and Southern Hispaniola contain Cretaceous volcanic units

| Massive veins | Massive veins | Massive veins | Massive veins | Massive veins | Massive veins | Massive veins | Massive veins | Massive veins | Massive veins | Massive veins | Massive veins | Massive veins | Massive veins | Massive veins | Massive veins |
|---|---|---|---|---|---|---|---|---|---|---|---|---|---|---|---|
| LP2-chromitite-4-14 | LP2-chromitite-4-16 | LP2-chromitite-4-18 | LP2-chromitite-4-24 | LP2-chromitite-4-34 | LP2-chromitite-4-40 | LP2-chromitite-4-41 | LP2-17-1-1 Line 004 | LP2-17-1-1 Line 007 | LP2-17-1-1 Line 010 | LP2-17-1-1 Line 023 | LP2-17-1-p13a-1 Line 7 | LP2-17-1-p13a-1 Line 10 | LP2-17-1-p13a-1 Line 19 | LP2-17-1-p13a-1 Line 21 | LP2-17-1-p13a-2 |
| 0.03 | b.d.l. | 0.04 | b.d.l. | 0.02 | b.d.l. | 0.04 | 0.03 | 0.02 | b.d.l. | b.d.l. | 0.03 | 0.02 | 0.05 | b.d.l. | b.d.l. |
| 1.10 | 0.92 | 1.06 | 1.25 | 1.16 | 0.89 | 1.13 | 0.67 | 0.69 | 0.78 | 0.87 | 0.68 | 0.82 | 0.74 | 0.85 | 0.97 |
| 12.51 | 12.53 | 12.22 | 11.98 | 11.92 | 12.97 | 13.17 | 11.05 | 12.28 | 12.61 | 11.53 | 12.62 | 12.70 | 11.08 | 11.61 | 11.65 |
| 48.03 | 48.03 | 48.52 | 48.84 | 48.44 | 49.18 | 48.27 | 52.73 | 52.20 | 50.61 | 50.57 | 52.12 | 50.70 | 51.52 | 50.79 | 50.69 |
| 17.31 | 16.36 | 17.37 | 17.47 | 16.51 | 17.52 | 17.43 | 19.67 | 19.31 | 18.95 | 19.43 | 19.47 | 19.37 | 19.28 | 19.46 | 19.24 |
| 8.41 | 9.45 | 8.25 | 7.90 | 8.58 | 6.94 | 7.46 | 5.44 | 5.46 | 6.47 | 7.38 | 5.23 | 6.23 | 7.23 | 7.26 | 7.41 |
| 0.37 | 0.33 | 0.37 | 0.37 | 0.34 | 0.33 | 0.36 | 0.22 | 0.21 | 0.19 | 0.22 | 0.16 | 0.19 | 0.23 | 0.18 | 0.20 |
| 10.90 | 11.52 | 10.75 | 10.78 | 11.32 | 10.73 | 10.94 | 9.01 | 9.58 | 9.80 | 9.40 | 9.56 | 9.62 | 9.42 | 9.49 | 9.71 |
| 0.31 | 0.31 | 0.30 | 0.35 | 0.31 | 0.19 | 0.29 | 0.26 | 0.30 | 0.37 | 0.38 | 0.29 | 0.37 | 0.30 | 0.34 | 0.36 |
| 0.08 | 0.12 | 0.19 | 0.12 | 0.13 | 0.17 | 0.15 | 0.19 | 0.17 | 0.17 | 0.16 | 0.18 | 0.15 | 0.16 | 0.12 | 0.18 |
| 99.05 | 99.58 | 99.06 | 99.08 | 98.73 | 98.92 | 99.24 | 99.28 | 100.23 | 99.94 | 99.93 | 100.34 | 100.19 | 100.01 | 100.08 | 100.40 |
| 0.00 | b.d.l. | 0.00 | b.d.l. | 0.00 | b.d.l. | 0.00 | 0.00 | 0.00 | b.d.l. | b.d.l. | 0.00 | 0.00 | 0.00 | b.d.l. | b.d.l. |
| 0.03 | 0.02 | 0.03 | 0.03 | 0.03 | 0.02 | 0.03 | 0.02 | 0.02 | 0.02 | 0.02 | 0.02 | 0.02 | 0.02 | 0.02 | 0.02 |
| 0.48 | 0.48 | 0.47 | 0.47 | 0.46 | 0.50 | 0.51 | 0.44 | 0.48 | 0.49 | 0.45 | 0.49 | 0.49 | 0.43 | 0.45 | 0.45 |
| 1.25 | 1.24 | 1.26 | 1.27 | 1.26 | 1.28 | 1.25 | 1.39 | 1.36 | 1.31 | 1.32 | 1.35 | 1.31 | 1.35 | 1.33 | 1.32 |
| 0.48 | 0.45 | 0.48 | 0.48 | 0.45 | 0.48 | 0.48 | 0.55 | 0.53 | 0.52 | 0.54 | 0.53 | 0.53 | 0.53 | 0.54 | 0.53 |
| 0.21 | 0.23 | 0.20 | 0.20 | 0.21 | 0.17 | 0.18 | 0.14 | 0.14 | 0.16 | 0.18 | 0.13 | 0.15 | 0.18 | 0.18 | 0.18 |
| 0.01 | 0.01 | 0.01 | 0.01 | 0.01 | 0.01 | 0.01 | 0.01 | 0.01 | 0.01 | 0.01 | 0.00 | 0.01 | 0.01 | 0.01 | 0.01 |
| 0.53 | 0.56 | 0.53 | 0.53 | 0.56 | 0.52 | 0.53 | 0.45 | 0.47 | 0.48 | 0.46 | 0.47 | 0.47 | 0.47 | 0.47 | 0.48 |
| 0.01 | 0.01 | 0.01 | 0.01 | 0.01 | 0.01 | 0.01 | 0.01 | 0.01 | 0.01 | 0.01 | 0.01 | 0.01 | 0.01 | 0.01 | 0.01 |
| 0.00 | 0.00 | 0.00 | 0.00 | 0.00 | 0.00 | 0.00 | 0.00 | 0.00 | 0.00 | 0.00 | 0.00 | 0.00 | 0.00 | 0.00 | 0.00 |
| 0.72 | 0.72 | 0.73 | 0.73 | 0.73 | 0.72 | 0.71 | 0.76 | 0.74 | 0.73 | 0.75 | 0.73 | 0.73 | 0.76 | 0.75 | 0.74 |
| 0.53 | 0.56 | 0.52 | 0.52 | 0.55 | 0.52 | 0.53 | 0.45 | 0.47 | 0.48 | 0.46 | 0.47 | 0.47 | 0.47 | 0.46 | 0.47 |
| 0.18 | 0.20 | 0.18 | 0.17 | 0.19 | 0.15 | 0.16 | 0.12 | 0.12 | 0.14 | 0.16 | 0.11 | 0.13 | 0.16 | 0.15 | 0.16 |
| 2.06 | 1.73 | 2.11 | 2.21 | 1.92 | 2.53 | 2.34 | 3.61 | 3.53 | 2.93 | 2.63 | 3.72 | 3.11 | 2.67 | 2.68 | 2.60 |
| *Estimated composition for parental melts* | | | | | | | | | | | | | | | |
| 12.08 | 12.09 | 11.96 | 11.85 | 11.83 | 12.27 | 12.35 | 11.43 | 11.98 | 12.12 | 11.65 | 12.12 | 12.16 | 11.44 | 11.69 | 11.71 |
| 1.29 | 1.09 | 1.25 | 1.46 | 1.35 | 1.06 | 1.33 | 0.82 | 0.84 | 0.93 | 1.03 | 0.83 | 0.99 | 0.90 | 1.01 | 1.14 |
| 1.21 | 1.07 | 1.23 | 1.23 | 1.10 | 1.27 | 1.24 | 1.65 | 1.56 | 1.50 | 1.55 | 1.59 | 1.57 | 1.53 | 1.55 | 1.49 |

related to the CLIP, rocks from ophiolitic sequences, Late Jurassic deep-marine oceanic sediments, and Cretaceous arc-related igneous and sedimentary rocks (Lewis and Draper, 1990; Draper and Lewis, 1991; Lewis et al., 1991, 2002; Lapierre et al., 1997, 1999; Escuder-Viruete et al., 2007a, 2010). The extent of these units is often limited by km-scale left-lateral NW–SE to WNW–ESE trending fault zones with late Cretaceous to Cenozoic movement (Hernáiz Huerta et al., 2000).

### 2.1. The Caribbean Large Igneous Province in the Dominican Republic

The CLIP formed in a period of voluminous magmatic activity related to mantle plumes during the Early and Late Cretaceous. It includes rocks erupted mainly during three distinct events: 124–112 Ma (Lapierre et al., 2000; Escuder-Viruete et al., 2007b); 94–83 Ma, which represents the main plume pulse activity (Kerr et al., 1997; Sinton et al., 1998; Hastie et al., 2008); and 80–72 Ma (Révillon et al., 2000). However, the CLIP volcanism was active until 63 Ma (Loewen et al., 2013). In the Dominican Republic, the volcanic units influenced by the Cretaceous Caribbean plume consist of enriched mid-ocean ridge basalts (E-MORB), transitional basalts and ocean island basalts (OIB), generally with high $TiO_2$ and MgO contents, and local picritic cumulates. These units form the Duarte Complex (Lewis et al., 1991; Lapierre et al., 1997, 2000; Lewis et al., 2002; Escuder-Viruete et al., 2007a,b), the Siete Cabezas Formation (Donnelly et al., 1990; Sinton et al., 1998), the Pelona–Pico Duarte Formation (Escuder-Viruete et al., 2011b), and the Dumisseau Formation in Haiti (Escuder-Viruete et al., 2016) (Fig. 1). The Duarte Complex is a large geological body located at the NE sector of the Cordillera Central in the Dominican Republic and records the Early Cretaceous phase of the CLIP (Escuder-Viruete et al., 2007a). Basalts from the Siete Cabezas Formation were extruded directly over the Duarte Complex between 69.0 ± 0.7 Ma and 68.5 ± 0.5 Ma (Sinton et al., 1998). Covering a large area of the Cordillera Central, the Pelona–Pico Duarte Formation is the result of both extrusive and intrusive magmatic activity at least during 79–68 Ma (Escuder-Viruete et al., 2011b). In SW Hispaniola (Haiti), the Dumisseau Formation has been interpreted as an emerged fragment of the CLIP that includes volcanic rocks of, at least, late Campanian age (~74 Ma; Escuder-Viruete et al., 2016).

### 2.2. Loma Caribe peridotite

The Dominican Loma Caribe peridotite is one of the ophiolite-related ultramafic rocks exposed along the northern margin of the Caribbean Plate (Lewis et al., 2006). The peridotite extends along a NW–SE oriented belt, approximately 4–5 km wide and 95 km long, in the Cordillera Central (Fig. 1). The Loma Caribe peridotite is bounded by the Siete Cabezas Formation and Duarte and Río Verde Complexes to the SSW, and the Maimón and Peralvillo Sur formations to the NNE (Draper and Lewis, 1991; Hernáiz Huerta et al., 2000; Lewis et al., 2000, 2002; Escuder-Viruete et al., 2002). The Río Verde Complex and the Maimón and Peralvillo Sur formations consist of (meta)volcanic rocks that record different magmatic stages of the island-arc development and evolution. The Maimón Formation contains island arc tholeiites (IAT) and boninites, while the Río Verde Complex consist of IAT and normal mid-ocean ridge basalts (N-MORB) transitional to IAT (Escuder-Viruete et al., 2006, 2010; Torró et al., 2016). Both units are Early Cretaceous in age and represent the incipient to more mature stages of the primitive Caribbean arc evolution, respectively. In contrast, the Late Cretaceous basalts of the Peralvillo Sur Formation originated during intra-arc rifting related to island-arc extension (Escuder-Viruete et al., 2007b, 2008). The Loma Caribe peridotite is intruded by E-MORB gabbros and dolerite dykes, which are interpreted to have been derived from sources unaffected by subduction. Their enriched trace element patterns seem to reflect subsequent back-arc spreading and off-axis magmatism influenced by the CLIP plume source (Escuder-Viruete et al., 2008).

Lewis and Jiménez (1991), Draper et al. (1996) and Escuder-Viruete et al. (2002) interpreted the Loma Caribe peridotite to be part of a

**Table 2**
Representative results of electron-microprobe analyses of accessory chromian spinel from the host peridotites. Complete data set can be found in Appendix B.

| | Accessory | Accessory | Accessory | Accessory | Accessory | Accessory | Accessory | Accessory | Accessory | Accessory | Accessory | Accessory | Accessory | Accessory |
|---|---|---|---|---|---|---|---|---|---|---|---|---|---|---|
| | Subhedral | Subhedral | Subhedral | Subhedral | Subhedral | Subhedral | Subhedral | Subhedral | Vermicular | Vermicular | Vermicular | Vermicular | Vermicular | Vermicular |
| | LP2-17-2-p1-5 | LP2-17-1-p11-1 | LP2-17-5-p2-2 | LP2-17-5-p3a-1 | LP2-17-5-p3a-11 | LP2-17-5-p7a-2 | LP2-17-6-p7-13 | LP2-17-6-p7-19 | RD-17-24-p2a-1 | RD-17-24-p2a-8 | RD-17-24-p2a-19 | RD-17-24-p8-2 | RD-17-24-p6-14 | RD-17-24-p6-16 |
| wt.% | | | | | | | | | | | | | | |
| $SiO_2$ | 0.04 | 0.03 | 0.03 | b.d.l. | 0.04 | b.d.l. | b.d.l. | b.d.l. | 0.03 | b.d.l. | 0.03 | 0.02 | 0.02 | 0.05 |
| $TiO_2$ | 0.14 | 0.24 | 0.46 | 0.34 | 0.61 | 0.28 | 0.37 | 0.47 | 0.10 | 0.07 | 0.03 | 0.08 | 0.00 | 0.00 |
| $Al_2O_3$ | 18.38 | 12.82 | 12.39 | 12.45 | 12.48 | 13.43 | 12.59 | 13.21 | 34.52 | 34.83 | 37.03 | 39.03 | 46.89 | 46.55 |
| $Cr_2O_3$ | 47.05 | 47.79 | 48.29 | 50.33 | 47.56 | 47.95 | 48.47 | 46.89 | 33.75 | 33.56 | 30.75 | 27.98 | 20.91 | 20.80 |
| FeO | 20.11 | 23.13 | 22.46 | 21.40 | 25.23 | 23.53 | 22.87 | 23.16 | 14.77 | 14.49 | 13.81 | 15.18 | 13.47 | 13.20 |
| $Fe_2O_3$ | 4.14 | 8.79 | 8.09 | 6.89 | 7.67 | 7.26 | 7.90 | 8.18 | 1.56 | 1.69 | 1.90 | 1.97 | 1.21 | 1.24 |
| MnO | 0.17 | 0.30 | 0.29 | 0.25 | 0.35 | 0.30 | 0.29 | 0.28 | 0.13 | 0.11 | 0.12 | 0.09 | 0.08 | 0.13 |
| MgO | 9.36 | 6.83 | 7.22 | 7.96 | 5.37 | 6.51 | 6.90 | 6.77 | 14.57 | 14.77 | 15.29 | 14.59 | 16.51 | 16.48 |
| NiO | 0.10 | 0.10 | 0.16 | 0.20 | 0.14 | 0.10 | 0.17 | 0.16 | 0.14 | 0.16 | 0.14 | 0.17 | 0.17 | 0.16 |
| ZnO | 0.28 | 0.35 | 0.29 | 0.29 | 0.60 | 0.44 | 0.43 | 0.38 | 0.18 | 0.23 | 0.26 | 0.37 | 0.38 | 0.39 |
| Total | 99.78 | 100.38 | 99.67 | 100.10 | 100.05 | 99.80 | 99.99 | 99.50 | 99.75 | 99.92 | 99.35 | 99.49 | 99.65 | 99.01 |
| apfu | | | | | | | | | | | | | | |
| Si | 0.00 | 0.00 | 0.00 | b.d.l. | 0.00 | b.d.l. | b.d.l. | b.d.l. | 0.00 | b.d.l. | 0.00 | 0.00 | 0.00 | 0.00 |
| Ti | 0.00 | 0.01 | 0.01 | 0.01 | 0.02 | 0.01 | 0.01 | 0.01 | 0.00 | 0.00 | 0.00 | 0.00 | 0.00 | 0.00 |
| Al | 0.70 | 0.50 | 0.49 | 0.49 | 0.50 | 0.53 | 0.50 | 0.52 | 1.18 | 1.19 | 1.26 | 1.32 | 1.52 | 1.52 |
| Cr | 1.20 | 1.26 | 1.28 | 1.32 | 1.27 | 1.27 | 1.28 | 1.25 | 0.78 | 0.77 | 0.70 | 0.63 | 0.45 | 0.46 |
| $Fe^{2+}$ | 0.54 | 0.65 | 0.63 | 0.60 | 0.72 | 0.66 | 0.64 | 0.65 | 0.36 | 0.35 | 0.33 | 0.36 | 0.31 | 0.31 |
| $Fe^{3+}$ | 0.10 | 0.22 | 0.20 | 0.17 | 0.20 | 0.18 | 0.20 | 0.21 | 0.03 | 0.04 | 0.04 | 0.04 | 0.03 | 0.03 |
| Mn | 0.00 | 0.01 | 0.01 | 0.01 | 0.01 | 0.01 | 0.01 | 0.01 | 0.00 | 0.00 | 0.00 | 0.00 | 0.00 | 0.00 |
| Mg | 0.45 | 0.34 | 0.36 | 0.39 | 0.27 | 0.33 | 0.34 | 0.34 | 0.63 | 0.64 | 0.66 | 0.62 | 0.68 | 0.68 |
| Ni | 0.00 | 0.00 | 0.00 | 0.01 | 0.00 | 0.00 | 0.00 | 0.00 | 0.00 | 0.00 | 0.00 | 0.00 | 0.00 | 0.00 |
| Zn | 0.01 | 0.01 | 0.01 | 0.01 | 0.02 | 0.01 | 0.01 | 0.01 | 0.00 | 0.00 | 0.01 | 0.01 | 0.01 | 0.01 |
| Cr# | 0.63 | 0.71 | 0.72 | 0.73 | 0.72 | 0.71 | 0.72 | 0.70 | 0.40 | 0.39 | 0.36 | 0.32 | 0.23 | 0.23 |
| Mg# | 0.45 | 0.34 | 0.36 | 0.40 | 0.27 | 0.33 | 0.35 | 0.34 | 0.64 | 0.64 | 0.66 | 0.63 | 0.69 | 0.69 |
| $Fe^{3+}$# | 0.07 | 0.16 | 0.15 | 0.14 | 0.14 | 0.13 | 0.15 | 0.15 | 0.02 | 0.02 | 0.03 | 0.02 | 0.01 | 0.01 |
| FeO/$Fe_2O_3$ | 4.86 | 2.63 | 2.78 | 3.11 | 3.29 | 3.24 | 2.90 | 2.83 | 9.45 | 8.57 | 7.28 | 7.72 | 11.10 | 10.60 |

Cations calculated on the basis of 32 oxygens; b.d.l. = below detection limit.

dismembered ophiolite obducted during the late Aptian, very likely as a result of the collision of an oceanic plateau (Duarte Complex) with the primitive Caribbean island arc (Maimón Formation), which represent the earliest stage of island arc magmatism within the Great Antilles Arc. Available structural data suggests N to NE-directed thrusting of the peridotite over the metavolcanic rocks of the Maimón Formation. Since their surface exposure, the peridotites have undergone extensive weathering and laterization processes that resulted in the formation of large Ni-laterite deposits currently mined (Villanova-de-Benavent et al., 2014; Aiglsperger et al., 2015). The analysis of unweathered samples of the Loma Caribe peridotites (<40% serpentinization; Haldemann et al., 1979; Proenza et al., 2007; Marchesi et al., 2016) reveals a predominance of clinopyroxene-bearing and spinel-bearing harzburgites over lherzolites, as well as the existence of small (<10 m across) lens-like and tabular bodies of dunites and orthopyroxene-bearing dunites hosted within harzburgites. Whole-rock composition of these lherzolites overlaps that of abyssal mantle peridotites from mid-ocean ridge (MOR) sources, whereas the spinel-bearing harzburgites and dunites are similar to those of refractory peridotites from a supra-subduction zone (SSZ) (Marchesi et al., 2016). Clinopyroxene-bearing harzburgites exhibit intermediate compositions that overlap those of residual mantle from both settings.

The compositional variations of the different types of peridotites record continued partial melting of different mantle sources in a MOR setting and during subsequent subduction initiation, enhanced by an increasing fluid influx from the subducting oceanic lithosphere (Marchesi et al., 2016). However, the peridotites are also intruded by late Cretaceous gabbroic and doleritic bodies with back-arc basin basalts (BABB) geochemical affinity, suggesting a later evolution in a back-arc tectonic environment (Escuder-Viruete et al., 2008, 2010). Therefore, the Loma Caribe peridotite records the transition from fore-arc towards back-arc settings.

### 2.3. Chromitite bodies

Small chromitite bodies (<10 m long) are hosted within peridotites in the northern and central part of the Loma Caribe peridotite belt (Fig. 1). These chromitite bodies are discontinuous lenses or pods, rarely exceeding 1 m in thickness, that are generally hosted in dunite exhibiting variable degrees of serpentinization (Fig. 2). Locally, chromitites from the central part of the peridotitic belt also occur as small veins (<2 cm thickness) which cross-cut both dunite and harzburgite (Fig. 2D).

The chromitites display typical massive textures (ca. 95 vol% chromian spinel). Chromite grains (Fig. 3) are unaltered and contain inclusions of both anhydrous (pyroxene) and hydrous (amphibole, serpentine, chlorite) silicates, and platinum-group minerals (PGM). The textural location and composition of these mineral inclusions are described in detail below. The primary silicate minerals from the matrix have been altered to chlorite and, to a lesser extent, serpentine. These minerals are accompanied by minute accessory pentlandite and awaruite (Proenza et al., 2007).

## 3. Samples and analytical procedures

Samples from the northern and central parts of Loma Caribe peridotite collected for this study include massive chromitite from individual pods ($n = 8$), the contact between the host peridotite and chromitite pods ($n = 7$), chromitite veins cross-cutting the peridotite ($n = 3$), and host peridotite with the lowest degree of serpentinization ($n = 1$). The samples were studied by optical and electron microscopy using an Environmental SEM Quanta 200 FEI, XTE 325/D8395 equipped with an INCA Energy 250 EDS microanalysis system at the *Centres Científics i Tècnics de la Universitat de Barcelona* (CCiTUB). Care was taken to identify unaltered zones of chromite, silicate and PGM inclusions suitable for in situ microanalysis. Major and minor elements in chromite and PGM were determined by electron microprobe analyses (EMPA) using a CAMECA SX-50 at the CCiTUB. Minor and trace elements in chromite were analyzed by laser ablation inductively coupled mass spectrometry (LA-ICP-MS) at the *Laboratorio de Estudios Isotópicos* (LEI) from the *Centro de Geociencias*, UNAM (Mexico), using a Resolution M − 50 Excimer laser coupled to a ThermoICap Qc ICP-MS. Analytical procedures for EMPA and LA-ICP-MS techniques are described in detail in Appendix A, and the results are presented in Tables 1–3 and 5.

Chromitite samples up to 500 g each from every single body sampled were crushed, sieved and processed using a hydroseparator (HS Lab, *Universitat de Barcelona*, Spain) to obtain concentrates of dense minerals. These mineral concentrates were later mounted as polished monolayers on resin blocks in order to identify platinum-group minerals (PGM) from the samples. Whole-rock PGE analyses were performed on 4 chromitite samples (3 from massive chromitite and 1 from a chromitite vein) at Genalysis Ltd (Perth, Western Australia). The analytical procedure is described in detail in Appendix A.

## 4. Results

### 4.1. Petrography

Massive chromitites display textures consisting of subhedral chromite grains with sizes from ~100 μm to 5 mm across (Fig. 3A). The smaller chromite grains are preferentially located at the contact with peridotite (Fig. 3B). Most of the samples exhibit a well-developed crack-seal network (Fig. 3C and D). Some fractures and some of the interstitial space between chromite grains are filled with serpentine, clinochlore and minor Ni–Fe–Cu sulfides and Fe–Ni alloys (Fig. 3E). Chromite grains are homogeneous, unaltered, with no chemical zoning except for weak retrograde effects along some fractures (Fig. 3D). Silicate, PGM and Ni–Cu sulfide inclusions are hosted within the chromite grains (Fig. 3F–H). Silicate inclusions are the most abundant and consist of primary pyroxene (enstatite) and late clinochlore and serpentine resulting from the alteration and serpentinization of the chromitite. The inclusions are generally subhedral, angular to rounded, with sizes up to 30 μm across. They are more abundant in the northern chromitite bodies, and occur with no preferential microstructural position or as clusters in the central part of chromite grains (Fig. 3G). Chromitite veins from the central chromitite deposits show the same textural features as those of the massive bodies but with smaller grain sizes ranging from ~100 μm to 1.5 mm.

Most of the peridotites hosting the chromitite bodies are dunites, but locally the chromitite veins cross-cut harzburgites. Both dunites and harzburgites are largely affected by serpentinization and no primary minerals are preserved, including accessory chromian spinel that appears completely altered and fractured displaying porous texture. Locally however, peridotites preserve relics of primary olivine, orthopyroxene, minor clinopyroxene and accessory chromian spinel (Figs. 2D and 3I–L). Olivine constitutes 1–3 mm euhedral grains with undulose extinction that occur as small patches surrounded by serpentine (mainly lizardite) (Fig. 3I). Orthopyroxene is porphyroclastic, 500 μm to 4 mm in size, with undulose extinction and locally displaying kink bands. Some grains show lobulated rims towards olivine indicative of resorption (Fig. 3J, L). Orthopyroxene contains thin exsolution lamellae of clinopyroxene oriented along its cleavage (Fig. 3J). Minor clinopyroxene also occurs as anhedral grains (up to 200 μm) associated with orthopyroxene and/or olivine. Locally, clinopyroxene is altered to secondary amphibole. Two types of accessory chromian spinel are observed in the peridotites. Relatively fresh subhedral chromian spinel grains, up to 150 μm long, occur close to the contact with the chromitite bodies generally within orthopyroxene and olivine grains (Fig. 3K). The other type of accessory chromian spinel is conspicuous further away from the contact with chromitites and consists of vermicular reddish grains

**Table 3**
Results of LA-ICP-MS analyses of chromite from the studied chromitites.

| Analysis | Location | Description | ppm | | | | | | | | | | | | | | | | |
|---|---|---|---|---|---|---|---|---|---|---|---|---|---|---|---|---|---|---|---|
| | | | $Al_2O_3$* | MgO* | FeO*t | $Cr_2O_3$* | V | int 2SE | LOD | Sc | int 2SE | LOD | Ga | int 2SE | LOD | Ti | int 2SE | LOD | Ni |
| LC-chr3c_C1_1 | Northern chromitites | Pods | 116900.0 | 124100.0 | 184400.0 | 557200.0 | 833.5 | 7.0 | 1.6 | −9.0 | 4.3 | 8.7 | 37.8 | 1.2 | 1.7 | 2010.0 | 49.0 | 32.6 | 1306.0 |
| LC-chr3c_C1_2 | Northern chromitites | Pods | 116900.0 | 124100.0 | 184400.0 | 557200.0 | 841.1 | 7.6 | 2.0 | −1.3 | 4.9 | 9.4 | 37.0 | 1.3 | 2.0 | 2093.0 | 51.0 | 32.9 | 1284.0 |
| LC-chr3c_C1_3 | Northern chromitites | Pods | 116900.0 | 124100.0 | 184400.0 | 557200.0 | 826.4 | 8.9 | 1.8 | 1.7 | 4.7 | 12.1 | 36.9 | 1.1 | 1.5 | 1981.0 | 54.0 | 20.9 | 1260.0 |
| LC-chr3c_C1_4 | Northern chromitites | Pods | 116900.0 | 124100.0 | 184400.0 | 557200.0 | 832.2 | 7.0 | 1.3 | −0.1 | 4.8 | 11.8 | 37.5 | 1.3 | 1.4 | 1981.0 | 48.0 | 38.1 | 1458.0 |
| LC-chr3c_C2_1 | Northern chromitites | Pods | 116900.0 | 124100.0 | 184400.0 | 557200.0 | 845.7 | 7.1 | 2.3 | 1.5 | 4.9 | 12.9 | 40.0 | 1.3 | 1.9 | 2060.0 | 54.0 | 28.9 | 1212.0 |
| LC-chr3c_C2_2 | Northern chromitites | Pods | 116900.0 | 124100.0 | 184400.0 | 557200.0 | 829.1 | 8.3 | 2.0 | 0.8 | 4.8 | 13.0 | 38.8 | 1.3 | 2.2 | 1969.0 | 54.0 | 35.7 | 1218.0 |
| LC-chr3c_C2_3 | Northern chromitites | Pods | 116900.0 | 124100.0 | 184400.0 | 557200.0 | 837.4 | 6.9 | 2.7 | 1.6 | 5 | 13.6 | 41.4 | 1.1 | 1.4 | 1993.0 | 50.0 | 35.6 | 1288.0 |
| LC-chr3c_C3_1 | Northern chromitites | Pods | 116900.0 | 124100.0 | 184400.0 | 557200.0 | 819.2 | 7.0 | 1.9 | 11.1 | 4.9 | 10.0 | 35.5 | 1.2 | 1.7 | 1954.0 | 50.0 | 36.9 | 1217.0 |
| LC-chr3c_C3_2 | Northern chromitites | Pods | 116900.0 | 124100.0 | 184400.0 | 557200.0 | 843.0 | 7.6 | 2.0 | 5.6 | 5.3 | 10.6 | 38.3 | 1.3 | 2.0 | 2002.0 | 47.0 | 40.8 | 1215.0 |
| LC-chr3c_C3_3 | Northern chromitites | Pods | 116900.0 | 124100.0 | 184400.0 | 557200.0 | 821.6 | 7.0 | 1.8 | 3.7 | 4.8 | 13.0 | 35.7 | 1.2 | 1.7 | 1928.0 | 50.0 | 29.8 | 1202.0 |
| LC-chr3c_C3_4 | Northern chromitites | Pods | 116900.0 | 124100.0 | 184400.0 | 557200.0 | 836.2 | 6.6 | 1.6 | 9.7 | 4.8 | 13.2 | 36.3 | 1.2 | 2.8 | 2016.0 | 53.0 | 38.6 | 1228.0 |
| LP1-m10_C1_1 | Central chromitites | Pods | 104600.0 | 92400.0 | 273500.0 | 514300.0 | 983.3 | 7.2 | 1.4 | 9.8 | 4.1 | 10.3 | 44.5 | 1.0 | 1.2 | 4417.0 | 68.0 | 21.5 | 4396.0 |
| LP1-m10_C1_2 | Central chromitites | Pods | 104600.0 | 92400.0 | 273500.0 | 514300.0 | 984.3 | 6.5 | 1.6 | 3.3 | 3.8 | 10.1 | 44.3 | 1.2 | 1.3 | 4387.0 | 69.0 | 30.4 | 4461.0 |
| LP1-m10_C1_3 | Central chromitites | Pods | 104600.0 | 92400.0 | 273500.0 | 514300.0 | 996.5 | 6.5 | 1.8 | 6.0 | 4.1 | 10.7 | 44.9 | 1.0 | 1.4 | 4432.0 | 67.0 | 23.0 | 4435.0 |
| LP1-m10_C1_4 | Central chromitites | Pods | 104600.0 | 92400.0 | 273500.0 | 514300.0 | 986.7 | 6.9 | 1.6 | 5.9 | 3.6 | 10.4 | 44.2 | 0.9 | 1.4 | 4508.0 | 69.0 | 35.8 | 4437.0 |
| LP1-m10_C2_1 | Central chromitites | Pods | 104600.0 | 92400.0 | 273500.0 | 514300.0 | 966.6 | 8.7 | 1.6 | 2.9 | 4 | 10.0 | 41.4 | 1.1 | 1.4 | 4044.0 | 71.0 | 26.1 | 3588.0 |
| LP1-m10_C2_2 | Central chromitites | Pods | 104600.0 | 92400.0 | 273500.0 | 514300.0 | 978.0 | 10.0 | 1.9 | 3.5 | 4 | 10.8 | 42.2 | 1.2 | 1.4 | 4258.0 | 66.0 | 22.6 | 3747.0 |
| LP1-m10_C2_3 | Central chromitites | Pods | 104600.0 | 92400.0 | 273500.0 | 514300.0 | 999.1 | 6.4 | 1.8 | 9.2 | 4.2 | 10.2 | 43.9 | 1.0 | 1.6 | 4429.0 | 78.0 | 23.1 | 3608.0 |
| LP1-m10_C3_1 | Central chromitites | Pods | 104600.0 | 92400.0 | 273500.0 | 514300.0 | 1050.5 | 8.6 | 1.8 | 1.8 | 4.1 | 12.9 | 44.9 | 1.2 | 1.9 | 4851.0 | 74.0 | 27.1 | 4579.0 |
| LP1-m10_C3_2 | Central chromitites | Pods | 104600.0 | 92400.0 | 273500.0 | 514300.0 | 994.8 | 7.4 | 1.6 | −1.4 | 4 | 10.2 | 42.2 | 1.1 | 1.4 | 4472.0 | 70.0 | 34.7 | 4253.0 |
| LP1-m10_C3_3 | Central chromitites | Pods | 104600.0 | 92400.0 | 273500.0 | 514300.0 | 1026.8 | 8.0 | 2.2 | 3.0 | 4.2 | 10.4 | 45.3 | 1.2 | 1.6 | 5146.0 | 80.0 | 29.7 | 3710.0 |
| LP1-m10_C3_4 | Central chromitites | Pods | 104600.0 | 92400.0 | 273500.0 | 514300.0 | 996.5 | 7.4 | 1.8 | −2.9 | 4.2 | 12.6 | 43.8 | 1.1 | 1.4 | 4334.0 | 75.0 | 29.1 | 3603.0 |
| LP2-17-5_C1_1 | Central chromitites | Veins | 121700.0 | 107900.0 | 242200.0 | 486100.0 | 1014.1 | 6.2 | 1.4 | 1.4 | 3.2 | 10.5 | 41.5 | 0.8 | 0.9 | 4156.0 | 51.0 | 15.7 | 2729.0 |
| LP2-17-5_C1_2 | Central chromitites | Veins | 121700.0 | 107900.0 | 242200.0 | 486100.0 | 988.5 | 6.7 | 2.5 | 2.6 | 3.2 | 9.5 | 41.9 | 0.8 | 0.9 | 3846.0 | 48.0 | 18.9 | 2701.0 |
| LP2-17-5_C1_3 | Central chromitites | Veins | 121700.0 | 107900.0 | 242200.0 | 486100.0 | 1015.7 | 7.5 | 3.4 | 10.1 | 4.2 | 12.9 | 40.4 | 1.0 | 1.5 | 4224.0 | 64.0 | 35.8 | 2499.0 |
| LP2-17-5_C1_4 | Central chromitites | Veins | 121700.0 | 107900.0 | 242200.0 | 486100.0 | 980.7 | 5.5 | 27.7 | 3.4 | 2.9 | 8.0 | 39.8 | 0.9 | 2.1 | 3916.0 | 46.0 | 99.5 | 2569.0 |
| LP2-17-5_C2_1 | Central chromitites | Veins | 121700.0 | 107900.0 | 242200.0 | 486100.0 | 1010.1 | 6.4 | 14.7 | 6.8 | 3.5 | 8.9 | 41.3 | 0.9 | 1.5 | 4048.0 | 56.0 | 50.9 | 2421.0 |
| LP2-17-5_C2_2 | Central chromitites | Veins | 121700.0 | 107900.0 | 242200.0 | 486100.0 | 1019.1 | 6.5 | 1.3 | −2.6 | 3.3 | 7.5 | 41.5 | 1.0 | 1.1 | 4038.0 | 62.0 | 18.3 | 2663.0 |
| LP2-17-5_C2_3 | Central chromitites | Veins | 121700.0 | 107900.0 | 242200.0 | 486100.0 | 1008.1 | 5.8 | 1.9 | −1.8 | 3.6 | 9.1 | 41.9 | 0.9 | 0.9 | 4252.0 | 58.0 | 28.3 | 2156.0 |
| LP2-17-5_C2_4 | Central chromitites | Veins | 121700.0 | 107900.0 | 242200.0 | 486100.0 | 994.9 | 6.8 | 2.0 | −4.9 | 3.3 | 12.2 | 40.4 | 0.9 | 1.7 | 3906.0 | 56.0 | 26.4 | 2464.0 |
| LP2-17-5_C3_1 | Central chromitites | Veins | 121700.0 | 107900.0 | 242200.0 | 486100.0 | 988.1 | 6.5 | 6.4 | −7.9 | 3.4 | 10.6 | 41.8 | 1.0 | 1.3 | 3777.0 | 49.0 | 29.3 | 2319.0 |
| LP2-17-5_C3_2 | Central chromitites | Veins | 121700.0 | 107900.0 | 242200.0 | 486100.0 | 1004.7 | 6.1 | 1.4 | 4.4 | 3.5 | 9.4 | 43.7 | 0.9 | 1.1 | 4601.0 | 59.0 | 18.4 | 2057.0 |
| LP2-17-5_C3_3 | Central chromitites | Veins | 121700.0 | 107900.0 | 242200.0 | 486100.0 | 967.4 | 6.1 | 1.3 | 15.3 | 3.7 | 9.7 | 40.9 | 0.9 | 1.1 | 3936.0 | 56.0 | 16.6 | 2105.0 |
| LP2-17-5_C3_4 | Central chromitites | Veins | 121700.0 | 107900.0 | 242200.0 | 486100.0 | 1044.3 | 7.4 | 1.1 | 6.5 | 3.4 | 9.4 | 43.5 | 1.0 | 1.0 | 4523.0 | 59.0 | 22.5 | 2069.0 |

(*) = Data from electron-microprobe; LOD = limit of detection; N=Normalized to chromite from MORB (Pagé and Barnes 2009).

(Fig. 3L). This second type is invariably associated with orthopyroxene and olivine.

### 4.2. Chromite mineral chemistry

For convenience, the chromian spinel in the chromitite and the host peridotite will be referred to as chromite. Electron microprobe analyses (Table 1) of unaltered primary chromite (<0.2 wt.% $SiO_2$) yield slightly heterogeneous $Cr_2O_3$ contents of 48.01–60.24 wt.%, the lower values being from the chromitite veins (Fig. 4A and B). The $Al_2O_3$ contents are more or less constant for the different bodies (~11 wt.%) and, consequently, all chromitites exhibit high Cr# [=Cr/(Cr + Al), atomic ratio = 0.71–0.83]. The Mg# [=Mg/(Mg + $Fe^{2+}$), atomic ratio] varies slightly from 0.44 to 0.61 (Fig. 4C). The studied chromitites are also systematically $TiO_2$-rich (ranging from 0.30 wt.% to 1.25 wt.%) compared to other high-Cr ophiolitic chromitites worldwide (Fig. 4B). The $Fe_2O_3$ contents are variable but consistently high, ranging between 2.77 wt.% and 9.16 wt.%, with $Fe^{3+}$# [=$Fe^{3+}$/($Fe^{3+}$+Cr + Al), atomic ratio] varying from 0.03 to 0.12. The two types of accessory chromite from the host peridotites show different compositions (Table 2). Subhedral chromite grains within orthopyroxene and olivine, which are systematically closer to the chromitite bodies, display high Cr# (0.62–0.75) and $Fe^{3+}$# (0.06–0.22), and low Mg# (0.27–0.41) values. They are also rich in $TiO_2$, with contents ranging from 0.24 wt.% to 0.72 wt.%. On the other hand, accessory vermicular chromite is Al-rich (Cr# = 0.22–0.40) with high Mg# values (0.61–0.69) and very low $Fe^{3+}$# (0.01–0.03). Unlike the other analyzed chromite types, it displays very low $TiO_2$ contents ranging from below detection limit to 0.14 wt.%.

LA-ICP-MS analyses (Table 3) of chromite from the chromitite bodies yielded minor- and trace-elements contents of: 36–45 ppm Ga, 819–1051 ppm V, 1202–4579 ppm Ni, 274–319 ppm Co, 1699–2410 ppm Mn, and 1047–1497 ppm Zn (Fig. 5). No major differences are observed between

| ppm | | | | | | | | | | | Normalized | | | | | | | | | | | |
|---|---|---|---|---|---|---|---|---|---|---|---|---|---|---|---|---|---|---|---|---|---|---|
| int 2SE | LOD | Zn | int 2SE | LOD | Co | int 2SE | LOD | Mn | int 2SE | LOD | $(Al_2O_3)_N$ | $(MgO)_N$ | $(FeO^t)_N$ | $(Cr_2O_3)_N$ | $(V)_N$ | $(Sc)_N$ | $(Ga)_N$ | $(Ti)_N$ | $(Ni)_N$ | $(Zn)_N$ | $(Co)_N$ | $(Mn)_N$ |
| 22.0 | 3.9 | 1095.0 | 38.0 | 7.6 | 278.8 | 4.4 | 1.8 | 1699.0 | 13.0 | 4.3 | 0.32 | 0.68 | 1.35 | 1.87 | 1.12 | 0.00 | 0.72 | 1.50 | 0.74 | 2.35 | 1.69 | 1.93 |
| 23.0 | 3.1 | 1086.0 | 38.0 | 7.2 | 273.5 | 4.5 | 1.7 | 1720.0 | 13.0 | 3.8 | 0.32 | 0.68 | 1.35 | 1.87 | 1.13 | 0.00 | 0.70 | 1.56 | 0.73 | 2.34 | 1.66 | 1.95 |
| 25.0 | 4.8 | 1084.0 | 29.0 | 6.0 | 274.9 | 5.0 | 1.4 | 1712.0 | 17.0 | 3.0 | 0.32 | 0.68 | 1.35 | 1.87 | 1.11 | 0.32 | 0.70 | 1.48 | 0.71 | 2.33 | 1.67 | 1.94 |
| 30.0 | 3.5 | 1210.0 | 33.0 | 12.2 | 279.5 | 4.6 | 1.3 | 2019.0 | 26.0 | 3.7 | 0.32 | 0.68 | 1.35 | 1.87 | 1.12 | 0.00 | 0.71 | 1.48 | 0.83 | 2.60 | 1.69 | 2.29 |
| 21.0 | 4.5 | 1241.0 | 32.0 | 6.3 | 282.8 | 4.8 | 1.8 | 1766.0 | 14.0 | 4.4 | 0.32 | 0.68 | 1.35 | 1.87 | 1.14 | 0.28 | 0.76 | 1.53 | 0.69 | 2.67 | 1.71 | 2.00 |
| 22.0 | 4.5 | 1126.0 | 35.0 | 8.0 | 281.9 | 4.9 | 2.6 | 1838.0 | 15.0 | 3.4 | 0.32 | 0.68 | 1.35 | 1.87 | 1.11 | 0.15 | 0.74 | 1.47 | 0.69 | 2.42 | 1.71 | 2.09 |
| 24.0 | 3.8 | 1112.0 | 33.0 | 6.7 | 283.3 | 4.5 | 1.9 | 1754.0 | 16.0 | 4.3 | 0.32 | 0.68 | 1.35 | 1.87 | 1.13 | 0.30 | 0.79 | 1.48 | 0.73 | 2.39 | 1.72 | 1.99 |
| 20.0 | 5.3 | 1094.0 | 31.0 | 8.7 | 279.1 | 4.9 | 1.7 | 1760.0 | 13.0 | 4.0 | 0.32 | 0.68 | 1.35 | 1.87 | 1.10 | 2.09 | 0.68 | 1.46 | 0.69 | 2.35 | 1.69 | 2.00 |
| 23.0 | 4.7 | 1063.0 | 34.0 | 5.3 | 286.4 | 4.5 | 2.3 | 1744.0 | 15.0 | 4.2 | 0.32 | 0.68 | 1.35 | 1.87 | 1.13 | 1.06 | 0.73 | 1.49 | 0.69 | 2.29 | 1.74 | 1.98 |
| 21.0 | 2.8 | 1096.0 | 32.0 | 9.2 | 274.1 | 5.4 | 2.1 | 1731.0 | 14.0 | 4.2 | 0.32 | 0.68 | 1.35 | 1.87 | 1.10 | 0.70 | 0.68 | 1.44 | 0.68 | 2.36 | 1.66 | 1.96 |
| 25.0 | 4.3 | 1047.0 | 30.0 | 9.1 | 276.1 | 5.0 | 1.2 | 1750.0 | 15.0 | 4.1 | 0.32 | 0.68 | 1.35 | 1.87 | 1.12 | 1.83 | 0.69 | 1.50 | 0.70 | 2.25 | 1.67 | 1.99 |
| 42.0 | 5.2 | 1442.0 | 39.0 | 10.6 | 317.9 | 4.4 | 1.5 | 2374.0 | 16.0 | 2.5 | 0.28 | 0.51 | 1.99 | 1.72 | 1.32 | 1.85 | 0.85 | 3.29 | 2.49 | 3.10 | 1.93 | 2.69 |
| 45.0 | 5.1 | 1473.0 | 35.0 | 7.3 | 316.3 | 4.7 | 1.4 | 2393.0 | 16.0 | 2.3 | 0.28 | 0.51 | 1.99 | 1.72 | 1.32 | 0.62 | 0.84 | 3.27 | 2.53 | 3.17 | 1.92 | 2.72 |
| 38.0 | 3.3 | 1403.0 | 36.0 | 6.9 | 314.7 | 4.9 | 1.1 | 2365.0 | 14.0 | 2.9 | 0.28 | 0.51 | 1.99 | 1.72 | 1.34 | 1.13 | 0.86 | 3.30 | 2.51 | 3.02 | 1.91 | 2.68 |
| 41.0 | 2.3 | 1445.0 | 37.0 | 5.7 | 315.6 | 4.3 | 1.4 | 2399.0 | 16.0 | 2.1 | 0.28 | 0.51 | 1.99 | 1.72 | 1.33 | 1.11 | 0.84 | 3.36 | 2.51 | 3.11 | 1.91 | 2.72 |
| 51.0 | 4.1 | 1437.0 | 38.0 | 8.0 | 315.3 | 4.9 | 1.8 | 2396.0 | 23.0 | 2.7 | 0.28 | 0.51 | 1.99 | 1.72 | 1.30 | 0.55 | 0.79 | 3.01 | 2.03 | 3.09 | 1.91 | 2.72 |
| 46.0 | 2.3 | 1433.0 | 42.0 | 9.3 | 313.8 | 5.0 | 1.6 | 2397.0 | 20.0 | 2.3 | 0.28 | 0.51 | 1.99 | 1.72 | 1.31 | 0.66 | 0.80 | 3.17 | 2.12 | 3.08 | 1.90 | 2.72 |
| 38.0 | 3.6 | 1433.0 | 35.0 | 6.5 | 307.9 | 4.5 | 1.6 | 2375.0 | 15.0 | 2.7 | 0.28 | 0.51 | 1.99 | 1.72 | 1.34 | 1.74 | 0.84 | 3.30 | 2.04 | 3.08 | 1.87 | 2.70 |
| 47.0 | 4.4 | 1497.0 | 44.0 | 8.1 | 317.3 | 5.3 | 1.5 | 2410.0 | 19.0 | 3.6 | 0.28 | 0.51 | 1.99 | 1.72 | 1.41 | 0.34 | 0.86 | 3.61 | 2.59 | 3.22 | 1.92 | 2.74 |
| 38.0 | 4.2 | 1468.0 | 41.0 | 8.4 | 318.3 | 5.0 | 1.4 | 2362.0 | 17.0 | 2.3 | 0.28 | 0.51 | 1.99 | 1.72 | 1.34 | 0.00 | 0.80 | 3.33 | 2.41 | 3.16 | 1.93 | 2.68 |
| 38.0 | 3.6 | 1491.0 | 40.0 | 8.0 | 315.0 | 4.3 | 2.3 | 2310.0 | 15.0 | 3.4 | 0.28 | 0.51 | 1.99 | 1.72 | 1.38 | 0.57 | 0.86 | 3.83 | 2.10 | 3.21 | 1.91 | 2.62 |
| 40.0 | 4.5 | 1460.0 | 38.0 | 7.1 | 319.2 | 4.1 | 1.8 | 2367.0 | 16.0 | 3.3 | 0.28 | 0.51 | 1.99 | 1.72 | 1.34 | 0.00 | 0.83 | 3.23 | 2.04 | 3.14 | 1.93 | 2.69 |
| 24.0 | 1.9 | 1270.0 | 32.0 | 8.3 | 293.9 | 4.1 | 1.3 | 2146.0 | 12.0 | 2.9 | 0.33 | 0.59 | 1.77 | 1.63 | 1.36 | 0.26 | 0.79 | 3.10 | 1.55 | 2.73 | 1.78 | 2.44 |
| 24.0 | 9.5 | 1268.0 | 33.0 | 15.4 | 288.7 | 3.5 | 1.2 | 2138.0 | 13.0 | 4.6 | 0.33 | 0.59 | 1.77 | 1.63 | 1.33 | 0.49 | 0.80 | 2.86 | 1.53 | 2.73 | 1.75 | 2.43 |
| 28.0 | 20.8 | 1198.0 | 26.0 | 18.2 | 292.1 | 4.6 | 2.1 | 2154.0 | 14.0 | 6.6 | 0.33 | 0.59 | 1.77 | 1.63 | 1.37 | 1.91 | 0.77 | 3.15 | 1.42 | 2.58 | 1.77 | 2.44 |
| 25.0 | 107.7 | 1263.0 | 27.0 | 111.9 | 292.3 | 3.5 | 10.6 | 2115.0 | 12.0 | 64.1 | 0.33 | 0.59 | 1.77 | 1.63 | 1.32 | 0.64 | 0.76 | 2.92 | 1.45 | 2.72 | 1.77 | 2.40 |
| 27.0 | 50.1 | 1300.0 | 34.0 | 40.5 | 300.5 | 3.7 | 7.8 | 2259.0 | 14.0 | 38.9 | 0.33 | 0.59 | 1.77 | 1.63 | 1.36 | 1.28 | 0.79 | 3.02 | 1.37 | 2.80 | 1.82 | 2.56 |
| 28.0 | 2.4 | 1381.0 | 35.0 | 8.6 | 298.9 | 4.1 | 1.3 | 2255.0 | 16.0 | 1.9 | 0.33 | 0.59 | 1.77 | 1.63 | 1.37 | 0.00 | 0.79 | 3.01 | 1.51 | 2.97 | 1.81 | 2.56 |
| 24.0 | 3.7 | 1354.0 | 33.0 | 8.8 | 298.5 | 3.7 | 1.4 | 2240.0 | 12.0 | 2.2 | 0.33 | 0.59 | 1.77 | 1.63 | 1.35 | 0.00 | 0.80 | 3.17 | 1.22 | 2.91 | 1.81 | 2.54 |
| 28.0 | 3.3 | 1307.0 | 31.0 | 12.0 | 294.8 | 4.4 | 1.5 | 2275.0 | 16.0 | 2.9 | 0.33 | 0.59 | 1.77 | 1.63 | 1.34 | 0.00 | 0.77 | 2.91 | 1.40 | 2.81 | 1.79 | 2.58 |
| 27.0 | 17.2 | 1347.0 | 31.0 | 20.0 | 296.4 | 4.0 | 3.5 | 2237.0 | 13.0 | 18.2 | 0.33 | 0.59 | 1.77 | 1.63 | 1.33 | 0.00 | 0.80 | 2.81 | 1.31 | 2.90 | 1.80 | 2.54 |
| 24.0 | 2.2 | 1322.0 | 30.0 | 8.6 | 293.3 | 4.0 | 1.4 | 2236.0 | 13.0 | 2.8 | 0.33 | 0.59 | 1.77 | 1.63 | 1.35 | 0.83 | 0.83 | 3.43 | 1.16 | 2.84 | 1.78 | 2.54 |
| 22.0 | 2.8 | 1261.0 | 34.0 | 10.0 | 289.4 | 4.3 | 1.4 | 2288.0 | 16.0 | 2.7 | 0.33 | 0.59 | 1.77 | 1.63 | 1.30 | 2.89 | 0.78 | 2.93 | 1.19 | 2.71 | 1.75 | 2.60 |
| 23.0 | 2.6 | 1302.0 | 32.0 | 7.0 | 294.7 | 4.1 | 1.2 | 2187.0 | 14.0 | 1.7 | 0.33 | 0.59 | 1.77 | 1.63 | 1.40 | 1.23 | 0.83 | 3.37 | 1.17 | 2.80 | 1.79 | 2.48 |

chromite from the pods and the veins. In all cases, chromitite presents intermediate compositions between chromite from boninites and those from mid-ocean ridge basalts (MORB) (Fig. 5).

**Table 4**
Concentrations (ppb) of platinum group elements in the studied chromitites.

| Sample | Type | Os | Ir | Ru | Rh | Pt | Pd |
|---|---|---|---|---|---|---|---|
| LP-11-005 | Pods | 537 | 467 | 970 | 107 | 237 | 10 |
| LP-11-006 | Pods | 363 | 374 | 793 | 84 | 243 | 11 |
| Chromitite 3 | Pods | 1084 | 787 | 1388 | 178 | 1096 | 15 |
| Chromitite 4 | Veins | 262 | 229 | 446 | 47 | 194 | 11 |
| **Anomalies**[a] | | | | | | | |
| LP-11-005 | Pods | | | | | 2.32 | |
| LP-11-006 | Pods | | | | | 2.56 | |
| Chromitite 3 | Pods | | | | | 6.78 | |
| Chromitite 4 | Veins | | | | | 2.73 | |

[a] Calculated according to the method of Garuti et al. (1997).

### 4.3. Bulk-rock contents of platinum-group elements

Bulk-rock PGE contents (1189–4548 ppb; Table 4) are higher than the average values from ophiolitic chromitites (<1000 ppb total PGE; Leblanc, 1991; Gervilla et al., 2005; Ismail et al., 2010). Chromitites from the veins systematically show lower values than those from the pods (Fig. 6). The chondrite-normalized PGE contents of the samples exhibit an enrichment in IPGE (Os, Ir and Ru) relative to PPGE (Rh, Pt and Pd), defining a negative slope typical for ophiolitic chromitites. However, unlike other ophiolitic chromitites, Os, Ir and Ru are poorly fractionated, describing a relatively flat pattern. Moreover, the patterns display a positive Pt anomaly (2.32–6.78) with respect to Rh and Pt, whereas other high-Cr chromitites exhibit lower Pt anomalies (<1; e.g., chromitites from Mayarí district, Cuba, Gervilla et al., 2005). The Pt anomaly together with the high PGE concentrations of the studied chromitites clearly illustrates the anomalous composition of the studied chromitites.

**Table 5**
Results of electron-microprobe analyses of PGM and base-metal minerals from the studied chromitites (b.d.l. = below detection limit).

| Sample | Mineral | Os (wt.%) | Ir (wt.%) | Ru (wt.%) | Pt (wt.%) | Pd (wt.%) | Rh (wt.%) | Fe (wt.%) | Ni (wt.%) | Cu (wt.%) | Co (wt.%) | S (wt.%) | As (wt.%) | Total (wt.%) |
|---|---|---|---|---|---|---|---|---|---|---|---|---|---|---|
| LC-17-1_10-1 | Os-rich laurite | 23.67 | 8.40 | 32.23 | b.d.l. | b.d.l. | 0.33 | 0.82 | 0.13 | 0.31 | 0.03 | 32.84 | b.d.l. | 98.76 |
| LC-17-1_3-1 | Os-rich laurite | 21.20 | 4.81 | 37.03 | b.d.l. | b.d.l. | 0.70 | 0.58 | 0.97 | 0.13 | b.d.l. | 33.31 | b.d.l. | 98.73 |
| LC-17-1_5-1 | Laurite | 11.78 | 3.18 | 47.94 | 0.20 | b.d.l. | b.d.l. | 0.09 | 0.13 | 0.19 | 0.03 | 35.47 | b.d.l. | 99.01 |
| LC-17-1_5-3 | Laurite | 12.75 | 3.26 | 46.55 | 0.26 | b.d.l. | 0.24 | 0.01 | 0.08 | 0.20 | b.d.l. | 35.43 | b.d.l. | 98.76 |
| LC-concentrate | Laurite | 18.48 | 8.23 | 37.29 | b.d.l. | 1.41 | 0.31 | 0.89 | 0.09 | 0.02 | 0.01 | 33.23 | 0.87 | 101.20 |
| LP2-concentrate | Laurite | 17.77 | 7.16 | 37.19 | b.d.l. | 1.35 | 1.21 | 0.90 | 0.01 | b.d.l. | 0.03 | 33.32 | 0.75 | 99.97 |
| LP1-concentrate | Zaccarinite | b.d.l. | 0.72 | 1.10 | b.d.l. | 0.02 | 43.63 | 0.32 | 25.03 | b.d.l. | b.d.l. | b.d.l. | 28.94 | 99.78 |
| LP1-concentrate | Ir–Fe–Ni alloy | 0.12 | 67.82 | 0.52 | 0.33 | b.d.l. | 0.10 | 17.33 | 11.94 | b.d.l. | 0.31 | b.d.l. | b.d.l. | 98.54 |
| LP1-concentrate | Ru–Os–Fe alloy | 24.75 | 11.60 | 41.86 | b.d.l. | 0.03 | 3.10 | 8.80 | 1.10 | b.d.l. | 0.22 | 0.01 | 0.38 | 92.72 |
| LC-concentrate | Pt–Ir–Fe–Ni alloy | b.d.l. | 4.28 | 0.09 | 50.49 | 0.15 | 0.55 | 12.96 | 17.58 | 0.91 | 0.03 | 0.01 | b.d.l. | 87.43 |
| LP2-concentrate | Pt–Fe alloy | b.d.l. | b.d.l. | b.d.l. | 86.79 | 0.16 | 0.33 | 9.89 | 0.28 | 0.42 | 0.05 | 0.02 | 0.04 | 98.19 |

### 4.4. PGM mineralogy

Platinum group minerals (PGM) were observed both in situ in thin sections and in mineral concentrates obtained after the hydroseparation process. The PGM are especially abundant in the northern chromitite bodies. Laurite is the most abundant PGM (Fig. 7A–C), often forming single-phase magmatic euhedral crystals (<10 μm across) enclosed in unaltered chromite and locally associated with millerite, Ir or Pt native elements (Fig. 7A and B). The chemical composition of magmatic laurite is dominated by the Ru–Os substitution, with minor Ir, Rh, Ni and Cu (up to 8.40, 1.21, 0.13, and 0.31 wt.%, respectively; Table 5). Similar compositions have been documented in laurite grains from chromitite bodies

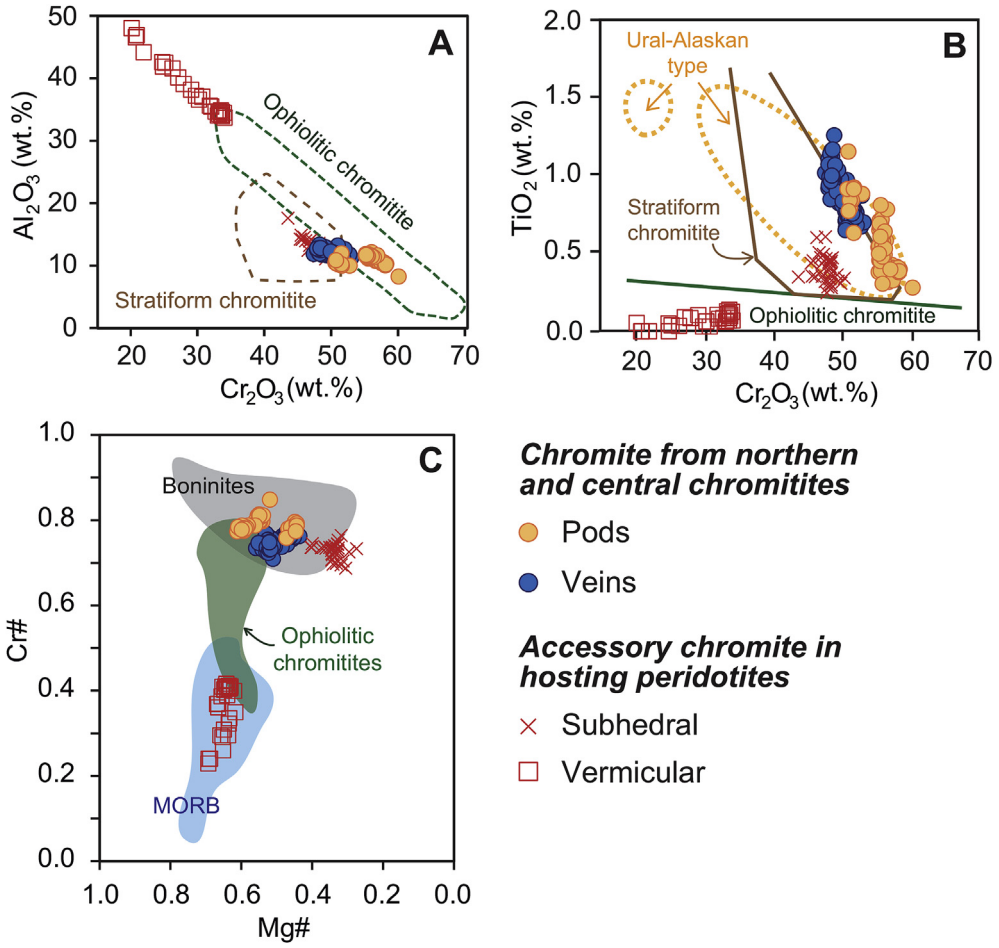


**Fig. 4.** Composition of primary chromite from the northern and central Loma Caribe peridotite compared to chromian spinel from various tectonic settings in terms of (A) $Al_2O_3$ vs. $Cr_2O_3$, (B) $TiO_2$ vs. $Cr_2O_3$, and (C) Cr# [=Cr/(Cr + Al), atomic ratio] vs. Mg# [=Mg/(Mg + $Fe^{2+}$), atomic ratio]. Data for chromian spinel of different tectonic settings are compiled from Bonavia et al. (1993), Kamenetsky et al. (2001), Proenza et al. (2007), and González-Jiménez et al. (2015).

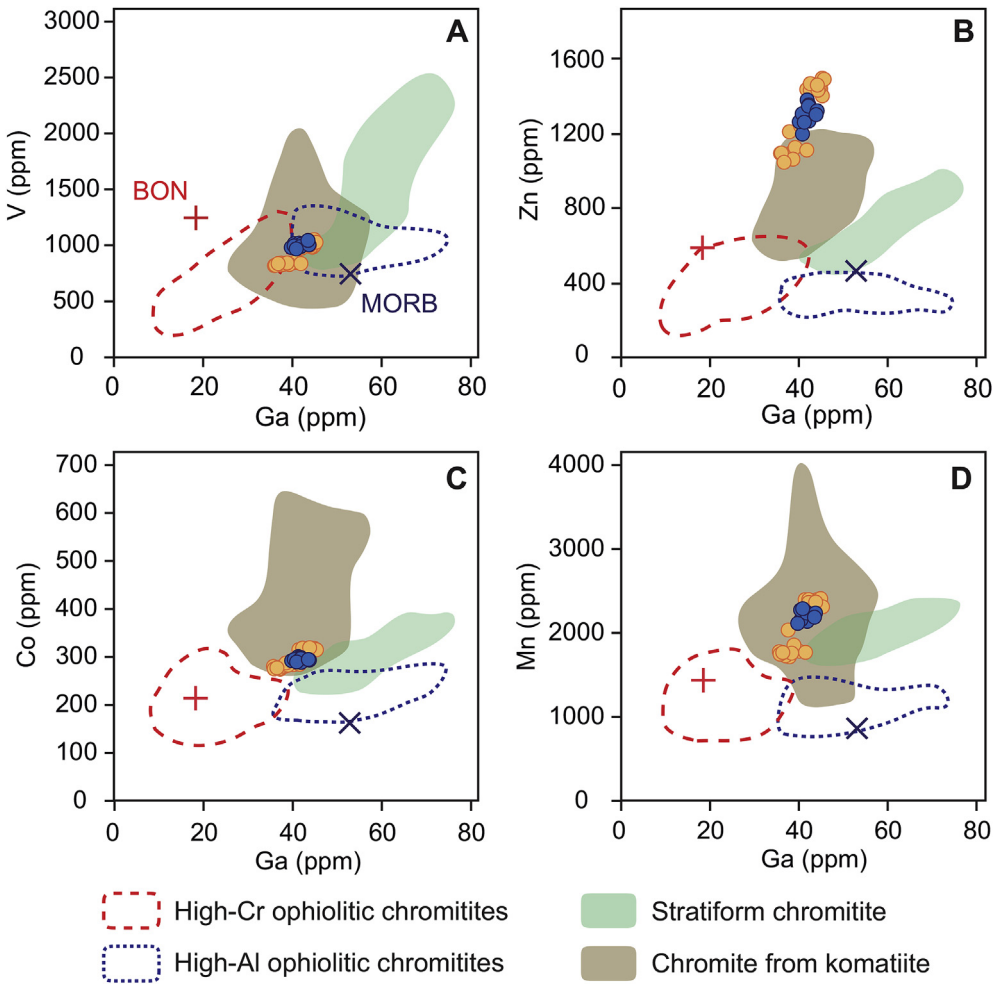


**Fig. 5.** Variations in terms of Ga vs. V, Zn, Co, and Mn of chromite from chromitites. Values of chromite from boninite (BON) lavas (red cross) and mid-ocean ridge basalt (MORB; blue cross) are from Pagé and Barnes (2009). Data sources of the other fields are listed in Appendix C. Symbols legend from Fig. 4.

of the central deposits of Loma Caribe peridotite (Proenza et al., 2007). Other PGM include Ru–Os–Fe alloys, and (Pt)–Ir–Fe–Ni alloys, often associated with zaccarinite (Figs. 7 and 8).

## 5. Discussion

### 5.1. Melts in equilibrium with chromitite: a comparison with plume-related erupted lava flows and other igneous rocks in the Dominican Republic

We have used the $Al_2O_3$ and $TiO_2$ composition of the studied chromitites to calculate the composition of their equilibrium melts using the approach of Kamenetsky et al. (2001) as modified by Zaccarini et al. (2011). The FeO/MgO ratios of the melts were also calculated from the chromite composition using the empirical formulation proposed by Maurel (1984). The calculations yield 10 wt.% to 12.42 wt.% $Al_2O_3$ and high $TiO_2$ (between 0.40 wt.% and 1.46 wt.%), with FeO/MgO ratios varying between 0.83 and 1.75 (Table 6). These compositions of the parental melt are different from those typically associated with the formation of high-Cr ophiolitic chromitites: boninitic melts are $TiO_2$-depleted (0.1–0.5 wt.%; Hicky and Frey, 1982) and Mg-rich (i.e., low FeO/MgO ratios) (e.g., Dick and Bullen, 1984; Kelemen et al., 2004). Rather, the composition of the calculated parental melt is closer to MORB in terms of $TiO_2$ and FeO/MgO (1.20–1.68 wt.% and 1.38, respectively; Gale et al., 2013). However, typical MORB has higher $Al_2O_3$ (15–16 wt.%) than those inferred for the Loma Caribe chromitites. The calculated $Al_2O_3$ values of the parental melt are also lower than in Cretaceous

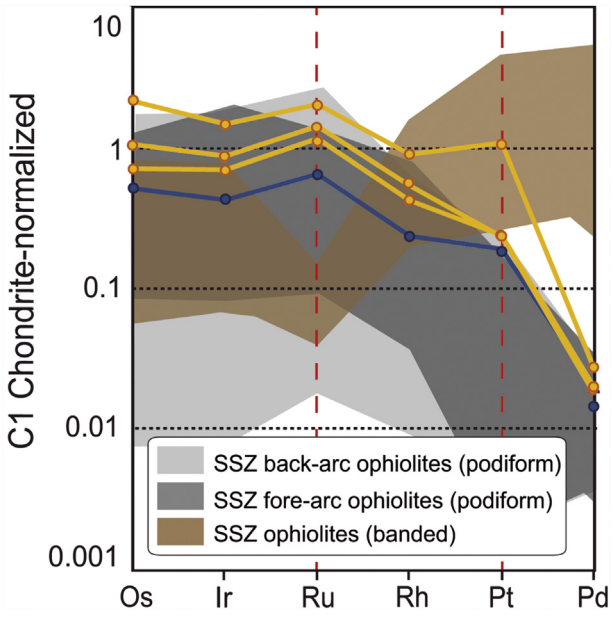


**Fig. 6.** C1 chondrite-normalized (Naldrett and Duke, 1980) patterns of Loma Caribe chromitites and comparison with other mantle-hosted chromitites. Data sources are Economou (1983), Pedersen et al. (1993), Melcher et al. (1997), Economou-Eliopoulos (2010), and Arai (2013), and references therein. Yellow symbols = chromitite pods; blue symbols = chromitite veins.

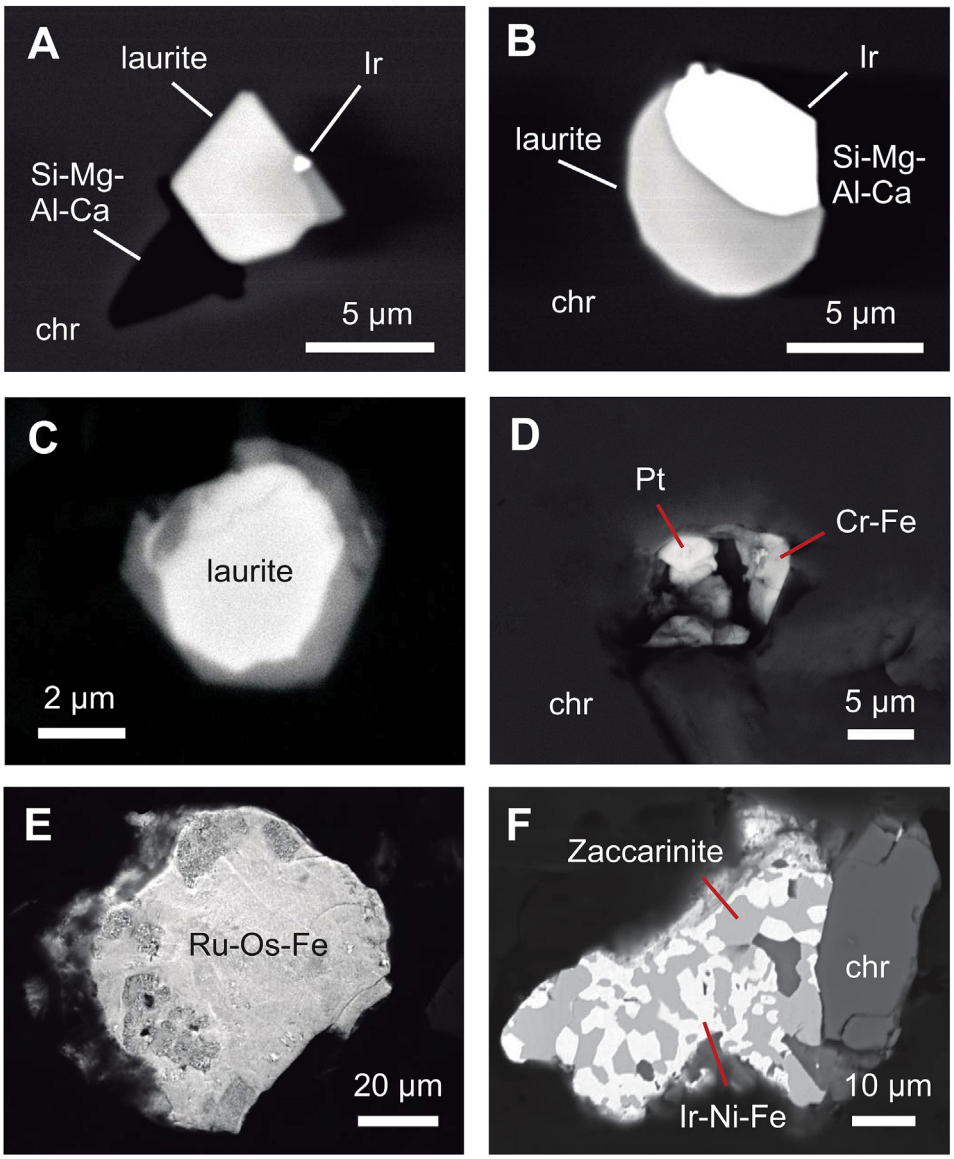


**Fig. 7.** Backscattered electron images of representative platinum-group mineral assemblages from the Loma Caribe chromitites. (A, B) Euhedral laurite grain associated with Ir alloy and a Si–Mg–Al–Ca mineral phase included in chromite. (C) Separated euhedral laurite grain. (D) Pt alloy associated with Cr–Fe alloy included in chromite. (E) Separated Ru–Os–Fe alloy grain with rugged surface. (F) Separated association of Rh–Ni–As and Ir–Ni–Fe alloys with chromite. chr = chromite.

volcanic arc basalts from the Dominican Republic (Table 6; Lewis et al., 2002; Escuder-Viruete et al., 2008, 2010). Nevertheless, these values are similar to basaltic rocks of the Duarte Complex and the Siete Cabezas Formation, which also fit the calculated $TiO_2$ contents. Picrites and high-Mg basalts from the Duarte Complex are Ti-rich (between 1.6 and 2.6 wt.% $TiO_2$) and show $Al_2O_3$ contents from 8.12 wt.% to 10.28 wt.% (Escuder-Viruete et al., 2007a). They also contain up to 1610 ppm Cr. Basalts from the Siete Cabezas Formation display 11.40–14.60 wt.% $Al_2O_3$ contents and are Ti-rich, ranging from 0.88 to 1.29 wt.% $TiO_2$ (Sinton et al., 1998; Escuder-Viruete et al., 2008). These basalts were derived from different source regions of a heterogeneous Caribbean mantle plume, responsible for the formation of the CLIP. Melts derived from different deep Caribbean plume enriched sources were incorporated by lateral flow and gave rise to OIB-like off-ridge magmatism in the back-arc area of the volcanic arc (Escuder-Viruete et al., 2007a, 2008, 2010).

The similarities between the inferred chromitites parental melts and the plume derived products of the Dominican Republic may account for an influence of the Caribbean plume in the chromitites parental melts mantle source. Moreover, plume-derived melts typically show higher Cr contents than island arc melts, and are more oxidized than melts associated with mid-ocean ridges and even subduction zones (Campbell, 2001; Ernst and Buchan, 2003; Mousallam et al., 2019). In addition, the mantle source of oceanic plateaus is thought to be PGE-richer than the source of normal mid-ocean ridge basalts (Ely and Neal, 2003).

### 5.2. *Interpretation of the geochemical signature of the chromitite*

Chromitites from the northern and central part of the Loma Caribe peridotite are high-Cr in composition (Cr# >0.7; Fig. 4C) but they are also systematically enriched in Ti (up to 1.25 wt.% $TiO_2$) and Ga (up to 45 ppm). This composition is very uncommon in high-Cr chromitites hosted in the mantle section of ophiolite complexes (Figs. 4B and 5; Pagé and Barnes, 2009; Zhou et al., 2014). The Ti contents of the studied chromitites are much higher than those reported in high-Cr chromitites hosted in the mantle section of ophiolites (<0.25 wt.% $TiO_2$; Leblanc and

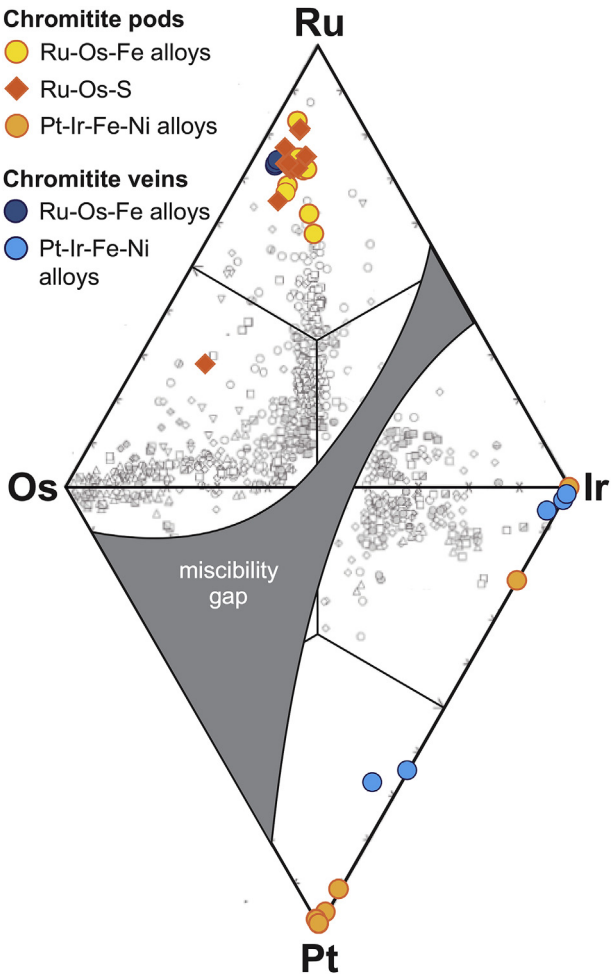


**Fig. 8.** Classification of the platinum group minerals found in the Loma Caribe chromitites in terms of Ru, Os, Ir, and Pt contents. Comparison data from Cabri (2002).

Nicolas, 1992; Rollinson et al., 2008), and also higher than those of high-Al chromitites located close to the mantle-crust transition zone of ophiolites (~0.5 wt.% $TiO_2$; Leblanc and Violette, 1983; Proenza et al., 1999; Zhou et al., 2001; Rollinson et al., 2008; Henares et al., 2010; González-Jiménez et al., 2014b; Arai and Miura, 2016). In the $Cr_2O_3$ versus $TiO_2$ plot of Fig. 4B, conventionally used to discriminate chromite from different tectonic settings, the studied chromites plot outside the compositional field of ophiolitic chromite. However, they overlap the field of chromites associated with layered mafic-ultramafic intrusions and Uralian-Alaskan type complexes. The lack of negative correlation between $Cr_2O_3$ and $TiO_2$ in the studied chromites evidences that their singularly high $TiO_2$ enrichment is not the result of progressive fractionation of a common parental melt, as observed in other mantle hosted chromitites (e.g., Proenza et al., 1999; Zaccarini et al., 2011). These observations indeed suggest that the parental melts of the studied chromitites derive from a mantle source different than that of ordinary ophiolitic chromitites. This is consistent with the fact that $TiO_2$ and $Al_2O_3$ contents of studied chromite plot in the fields of chromite in equilibrium with island arc basalts (IAB) and ocean island basalts (OIB) and the oceanic plateaus (Fig. 9; Tokuyama and Batiza, 1981; Kamenetsky et al., 2001).

Further insight on the nature of the parental melt of chromitites can be extracted from analyzing the concentration of minor and trace elements (e.g., Ga, V, Zn, Co, Mn) in chromite. For example, Ga has been proven to be a useful tool for fingerprinting the nature of the parental

**Table 6**
Composition of melts in equilibrium with chromite and of plume-related erupted lava flows and other igneous rocks in the Dominican Republic in terms of $Al_2O_3$ and $TiO_2$ contents (wt.%) and FeO/MgO ratios. Composition of melt in equilibrium with chromite from Loma Caribe chromitites has been calculated using values obtained from EMPA analyses. References: Boninite = Hicky and Frey (1982); MORB = Gale et al., 2013; Wilson, 1989; plume derived products and volcanic arc basalts = Lewis et al. (2002), Escuder-Viruete et al. (2008). IAT = island arc tholeiite; N-MORB = normal mid-ocean ridge basalt.

| | $Al_2O_3$ (wt.%) | $TiO_2$ (wt.%) | FeO/MgO |
|---|---|---|---|
| *Melts in equilibrium with chromite* | | | |
| Loma Caribe chromitites | 10–12.42 | 0.40–1.46 | 0.83–1.75 |
| Boninite | 10.6–14.4 | 0.1–0.5 | 0.7–1.4 |
| MORB | 15–16 | 1.20–1.68 | 1.38 |
| *Plume derived products* | | | |
| Duarte Complex (picrites, high-Mg basalts) | 8.12–10.28 | 1.6–2.6 | |
| Siete Cabezas Formation (basalts) | 11.40–14.60 | 0.88–1.29 | |
| *Volcanic arc basalts* | | | |
| Maimón Formation (IAT, boninites) | 14.2–16.24 | 0.47–0.99 | |
| Río Verde Complex (IAT, N-MORB) | 15.32–16.48 | 1.05–1.13 | |

melts of chromitite because it is unlikely to change during cooling and subsolidus processes (Dare et al., 2009; Pagé and Barnes, 2009; González-Jiménez et al., 2015; Derbyshire et al., 2019). The concentration of Ga from the studied chromite is higher than in chromite from other high-Cr ophiolitic chromitites. For ophiolitic chromitites, there is a general negative correlation between Cr# and Ga contents in chromite (e.g., Pagé and Barnes, 2009). As a result, high-Cr ophiolitic chromitite tends to be relatively impoverished in Ga (<30 ppm; Pagé and Barnes, 2009; Colás et al., 2014; Zhou et al., 2014; Eliopoulos and Eliopoulos, 2019), whereas higher Ga contents are usually related to high-Al ophiolitic chromitite (>40 ppm; Pagé and Barnes, 2009; Colás et al., 2014, 2019; Zhou et al., 2014; Eliopoulos and Eliopoulos, 2019). Eliopoulos and Eliopoulos (2019) also showed a positive trend between $Fe^{3+}$# in chromite and their Ga content. Therefore, the high Ga concentrations observed for the Dominican high-Cr ophiolitic chromitites could be linked to their consistent high $Fe_2O_3$ contents. In the studied chromite, Ga shows positive correlations with other trace elements (V, Zn, Co and Mn; Fig. 5) and the composition of chromite either overlaps the fields of high-Cr and high-Al chromitites or plots outside these two fields. Noteworthy, the analyzed chromites exhibit a trace element composition that overlaps the field of komatiitic chromite (Fig. 5). Interestingly, these chromite-bearing komatiites are associated with large igneous provinces (LIPs) caused by melting of hot plumes from the deep mantle (e.g., Richards et al., 1989; Campbell and Griffiths, 1990). Moreover, in spidergrams from Fig. 10, the trace element distribution of chromite displays characteristic positive anomalies in Ti and Ga similar to those of chromite in komatiites (Fig. 10C). Overall, the patterns resemble those of chromite from intraplate settings and clearly differ from the patterns defined by typical chromite from SSZ settings.

On the other hand, accessory chromite from the peridotite hosting the chromitites exhibits the typical subhedral morphology of cumulate chromites precipitated from percolating magmas in the mantle (Matsumoto and Arai, 2001). Interestingly, these grains show similar compositions in terms of Cr# and $TiO_2$ to the associated massive chromitites, also plotting outside the compositional field of ophiolitic chromitites (Fig. 4) but resembling that of island arc basalts, OIB and oceanic plateaus in terms of $TiO_2$ and $Al_2O_3$ (Fig. 9A) and Cr–Al–$Fe^{3+}$ (Fig. 9B). The composition of this type of accessory chromite, together with its proximity to the chromitite bodies, suggests that it formed from the same parental melt, although the lower Mg# indeed reflects subsolidus re-equilibration with the host orthopyroxene and/or olivine (e.g., Pagé and Barnes, 2009). In contrast, accessory chromite exhibiting

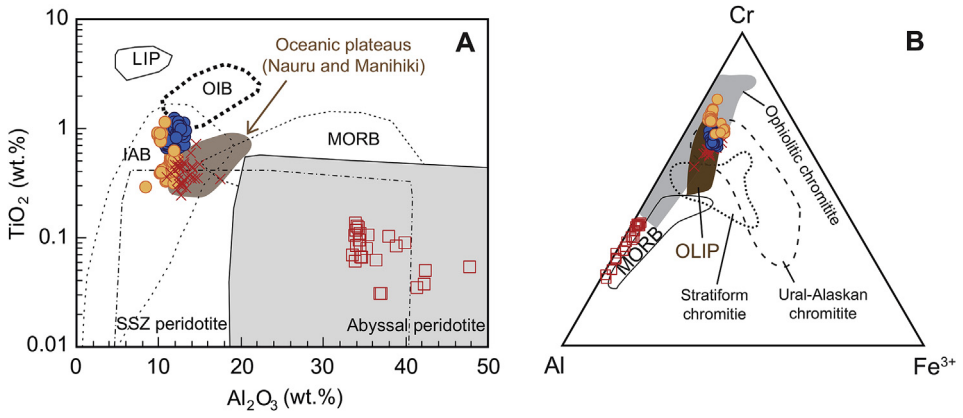


**Fig. 9.** Chemical composition of Loma Caribe chromite compared to chromite from volcanic and plutonic complexes from different geotectonic settings in terms of: (A) $TiO_2$ vs. $Al_2O_3$, and (B) Cr–Al–$Fe^{3+}$ compositions. Data compilation from Proenza et al. (2007) and Zhang et al. (2017). Symbols legend from Fig. 4. LIP = large igneous province; OIB = ocean island basalt; IAB = island arc basalt; MORB = mid-ocean ridge basalt; SSZ = supra-subduction zone.

vermicular-like morphology is compositionally distinct from chromite forming the chromitite bodies. Consistently, this chromite displays higher $FeO/Fe_2O_3$ ratio (>7) than the subhedral accessory chromite (<6) (Table 2), as is typical of restitic spinels in peridotites (Lenaz et al., 2000; Kamenetsky et al., 2001) with composition akin to chromite from MOR and abyssal settings (Fig. 9A and B). This vermicular chromite likely corresponds to the accessory chromite from the Loma Caribe clinopyroxene-harzburgite described by Marchesi et al. (2016), which, according to these authors, shows abyssal (ocean ridge) and supra-subduction zone compositions.

Summarizing, high-Cr chromitites from the northern and central Loma Caribe peridotite do not show the chemical signature of typical high-Cr chromitites hosted in the mantle section of ophiolites. Rather they exhibit major, minor and trace element fingerprints resembling those of chromite crystallized from melts evolved from mantle plumes, in contrast to the MORB or BABB character of residual vermicular-like chromite of the host peridotite. These mixed signatures reflect complex mechanism of chromitite formation.

### 5.3. Origin of the PGE signatures in the Dominican Republic chromitites

The distribution of the PGE in the mantle peridotites is mainly controlled by accessory base-metal minerals (BMM), including sulfides and refractory platinum-group minerals (PGM) (O'Driscoll and González-Jiménez, 2016, and references therein). Magmatic processes, such as partial melting and melt-rock reaction associated with upward migration of deep-sourced melts, promote destabilization of the PGE-bearing minerals, contributing to increase the budget of precious metals in basaltic melts. Under moderate degrees of mantle melting (<20%), the most refractory PGE (IPGE: Os, Ir, Ru) behave as compatible elements, while the less refractory PGE (PPGE: Pt and Pd), Au, Re, S, Se, Te and Cu are incompatible (Bockrath et al., 2004; Helmy et al., 2010; Fellows and Canil, 2012; König et al., 2012; González-Jiménez et al., 2014a; Saunders et al., 2015; Aulbach et al., 2016; Luguet and Reisberg, 2016). However, in the critical melting interval of 20%–25%, and depending on sulfur abundance and pressure (Mavrogenes and O'Neill, 1999), even the most refractory IPGE can be extracted from the mantle source and be diluted in the extracted melt (Luguet et al., 2003; Lorand and Grégoire, 2006; Prichard et al., 2008). Higher PGE contents and higher Cr# are expected with increasing degree of partial melting of the mantle source. Therefore, the observation that the studied chromitites exhibit a PGE enrichment and high-Cr composition supports: (1) a close genetic link between PGE abundances and the nature of the parental melts, and (2) that the Cr- and PGE-rich chromitites from the northern and central Loma Caribe peridotite deposits were precipitated from a PGE-rich magma generated by a high-degree of partial melting within the aforementioned interval (Arai and Yurimoto, 1994; Arai and Abe, 1995; Gervilla et al., 2005; Uysal et al., 2009; González-Jiménez et al., 2011). Moreover, the total PGE contents and the IPGE and PPGE proportions of the studied chromitites differ from chromitites from other contexts (Fig. 11), indicating that they formed from melts formed in a different geodynamic context than other well-known ophiolitic chromitites.

On the other hand, the geochemical PGE signature of the chromitites has a mineralogical expression in the suite of platinum-group minerals (PGM). On the basis of their textural position and composition, the PGM identified can be divided into primary and secondary phases. Thus, laurite grains included in chromite grains are considered primary, formed at the high-temperature magmatic stage before and during crystallization of chromite (Fig. 7A and B). In contrast Ru–Os–Fe and Pt–Ir–Fe–Ni alloys exhibiting rugged textures and located in fractures and edges of chromite grains are interpreted as secondary in origin, very likely originated by alteration of pre-existing magmatic PGM initially included in chromite (Fig. 7E). The abundance of laurite in chromite can be linked with the "collector" effect of this mineral during crystallization from mantle melts. According to experimental results, this effect can be related to the local reduction of oxygen fugacity ($fO_2$) at the edges of growing chromite crystals, which may trigger saturation of the most refractory and easily oxidized PGE (Os, Ir, Ru) originally dissolved in the melt (Gervilla et al., 2005; Mungall, 2005; Ballhaus et al., 2006; Finnigan et al., 2008; González-Jiménez et al., 2014a,b). In this model, the crystallizing chromite grains provide a nucleation substrate for nano-to micron-sized PGM (O'Driscoll and González-Jiménez, 2016, and references therein), promoting fractionation of the PGEs from the silicate melt. Recent experimental data by Anenburg and Mavrogenes (2016) suggest that this role of chromite as a physical collector of precious metals may not only apply to IPGE but also to Pt. At moderate to high $fO_2$ conditions, the solubility of Pt in the melt is strongly dependent on $fO_2$ (Cottrell and Walker, 2006; Médar et al., 2015). According to experimental studies, reduction of the melt can lead to Pt oversaturation and hence the formation of Pt-rich alloy nanoparticles (Amossé et al., 2000; Borisov and Palme, 2000; Ballhaus et al., 2006; Médar et al., 2015). In the case of the studied chromitites, we propose that precipitation of $Fe_2O_3$-rich chromite locally decreased $fO_2$ of the residual parental melt and enhanced the precipitation of the dissolved Pt as minute alloys (Fig. 7). This would explain the observed singular positive Pt anomaly (Fig. 6), generally uncommon in ophiolitic chromitites. Some authors attribute positive Pt anomalies observed in ophiolitic chromitites as the result of PGE local remobilization due to serpentinization (Graham et al., 1996). However, the presence of Pt alloys and Pt native element associated with primary laurite in the studied chromitites suggest that their Pt anomaly might reflect the primary platinum group mineralogy of the chromitites.

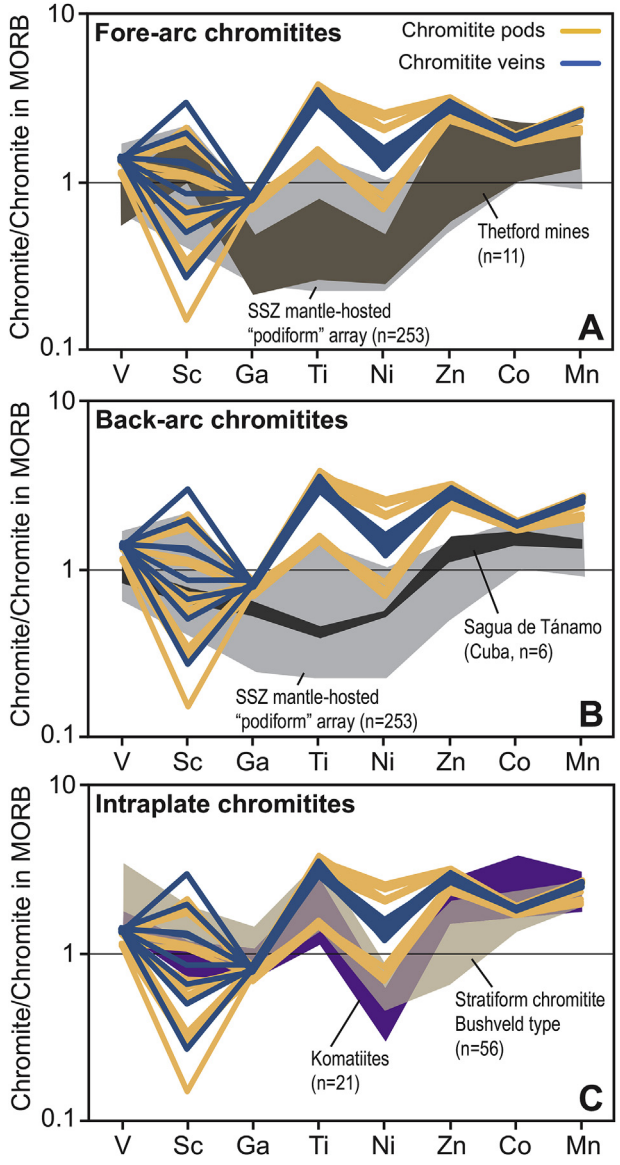


**Fig. 10.** Spider diagrams showing the composition of minor and trace elements of chromite from the Loma Caribe chromitites. Comparison with representative supra-subduction zone (SSZ) mantle-hosted high-Cr chromitites from (A) fore-arc and (B) back-arc regions and (C) with chromites in komatiites and from stratiform chromitites. Data sources for Thetford Mines and Sagua de Tánamo are Pagé and Barnes (2009) and González-Jiménez et al. (2015), respectively. Data sources for chromitites from the SSZ mantle-hosted podiform chromitite array, komatiites and stratiform chromitites (Bushveld-type) as in Fig. 5.

### 5.4. *Genesis of chromitites by peridotite–plume melt interactions in a back-arc tectonic environment*

#### 5.4.1. *Geodynamic framework of Loma Caribe mantle section*

The geochemical characteristics of the Loma Caribe peridotites observed by Marchesi et al. (2016) suggest a supra-subduction zone (SSZ) geodynamic setting. These authors proposed that the peridotites record mantle evolution during subduction initiation by the late Early Cretaceous. However, the presence of gabbroic bodies and dolerite dykes with geochemical signatures akin to BABB and E-MORB intruding the peridotites suggests a later development in a Late Cretaceous back-arc basin (Escuder-Viruete et al., 2008, 2010). On the basis of these observations, we suggest that the Loma Caribe mantle section underwent a multi-stage evolution during island-arc formation and evolution in the northern Caribbean plate margin.

The formation of the northern Caribbean island started in the Early Cretaceous, when SW-dipping subduction initiation of the proto-Caribbean oceanic basin took place (Pindell et al., 2012 and references therein). Fluids released by the slab promoted partial melting in the SSZ mantle wedge giving place to boninitic and tholeiitic to calc-alkaline magmas (e.g., Maimón–Amina and Los Ranchos formations, as well as the Río Verde Complex; Escuder-Viruete et al., 2008, 2010; Torró et al., 2017). The geochemical heterogeneity of the Loma Caribe mantle peridotites (i.e., lherzolites, clinopyroxene-harzburgites, harzburgites, orthopyroxene-dunites, and dunites) records the shifting conditions of melting during the development of the subduction zone (Marchesi et al., 2016). On the other hand, Escuder-Viruete et al. (2008, 2011) proposed a tectonomagmatic model involving intra-Caribbean island-arc rifting and back-arc basin development in the Late Cretaceous. Following this model, the Caribbean island-arc extension started at 90–88 Ma, causing stretching and thinning of the lithosphere, which rifted near the rheologically weak volcanic front. Increased thinning and rifting promoted the development of an intra-arc/back-arc basin with an incipient seafloor-spreading center. With the changing tectonic conditions, the location of the Loma Caribe peridotite shifted to a back-arc setting, where an adventive mantle system similar to that of mid-ocean ridges was progressively superimposed to the SSZ corner flow field (Gribble et al., 1998; Martínez and Taylor, 2002) and, consequently, BABB-like magmas extruded (e.g., Velazquitos gabbros and Peralvillo Sur Formation basalts; Escuder-Viruete et al., 2008). With continued extension and migration of the Caribbean island-arc towards the NE, at 85–80 Ma the magmatism of the seafloor spreading system may not have been significantly affected by slab-derived geochemical components. Moreover, during this process, the rollback of the SW-dipping subduction slab generated lateral mantle flow from the SW influenced by the Caribbean plume (Fig. 12; Escuder-Viruete et al., 2008, 2011b). During the Late Cretaceous (90–80 Ma), upwelling of this enriched mantle towards the spreading center and melting at low-P conditions likely produced E-MORB dolerite dykes intruding the Loma Caribe peridotite and the Campanian extrusion of Siete Cabezas Formation basalts in the NE sector of the Cordillera Central (Escuder-Viruete et al., 2008). Other units with plume-related rocks located in the Cordillera Central, the Pelona–Pico Duarte and Dumisseau formations, also contain off-axis OIB- and E-MORB-type magmatism derived from a deeper and more enriched Caribbean plume source (Escuder-Viruete et al., 2011b, 2016).

#### 5.4.2. *Genesis of chromitites*

As noted above, the composition (major and trace elements, including PGE) of the high-Cr chromitite bodies of Loma Caribe strongly suggest precipitation from melts derived from an enriched peridotite source influenced by a plume. In addition, the textural and chemical differences between subhedral and vermicular accessory chromite of the host peridotites indicate different origins: subhedral chromite crystallized from the same parental magma as the chromitites, whereas vermicular chromite is a restitic abyssal component of the peridotite. The occurrence of these two types of chromite in the same rocks implies that there was no chemical equilibrium between the chromitite-forming melt and their host peridotites. This is consistent with the intrusive character of the chromitites, as evidenced by their intrusion into both dunites and harzburgites (Fig. 2) and the decrease in chromite grain size towards the contact with the host peridotites (Fig. 3). We propose that chromitites from the northern and central parts of the Loma Caribe peridotite formed when their host peridotites where located at the back-arc basin at the rear of the Late Cretaceous volcanic Caribbean arc (Fig. 12). In this setting, the mantle source of the parental melts was not affected by slab-derived geochemical components but was modified by SW lateral flow from the Caribbean plume. The genesis of the Loma Caribe peridotite chromitites in this context can be conceptualized within the framework of previous models of ophiolitic chromitite formation. The chromitite parental melts were channelized and latter emplaced within pre-existing dunite bodies, which represent high-porosity and high-permeability channels (Braun

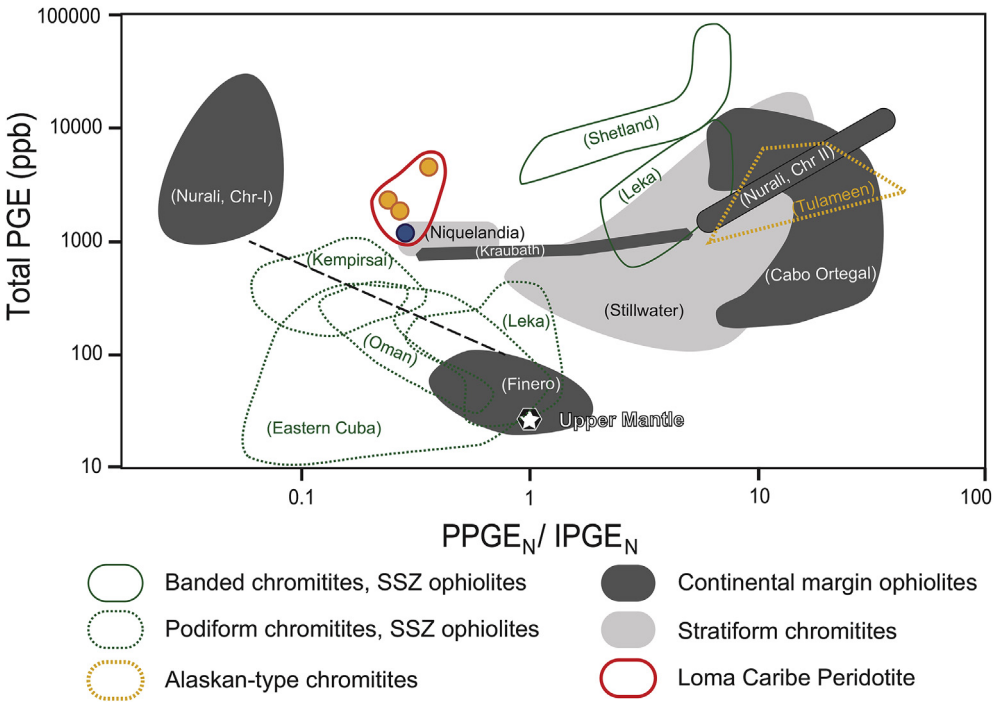


**Fig. 11.** Chondrite-normalized PPGE/IPGE vs. ΣPGE in chromitite and related ultramafic and mafic rocks. Modified after Melcher et al. (1999). Dotted line corresponds to the ophiolitic trend (compilation from Saha et al., 2018). Yellow symbols = chromitite pods; blue symbols = chromitite veins.

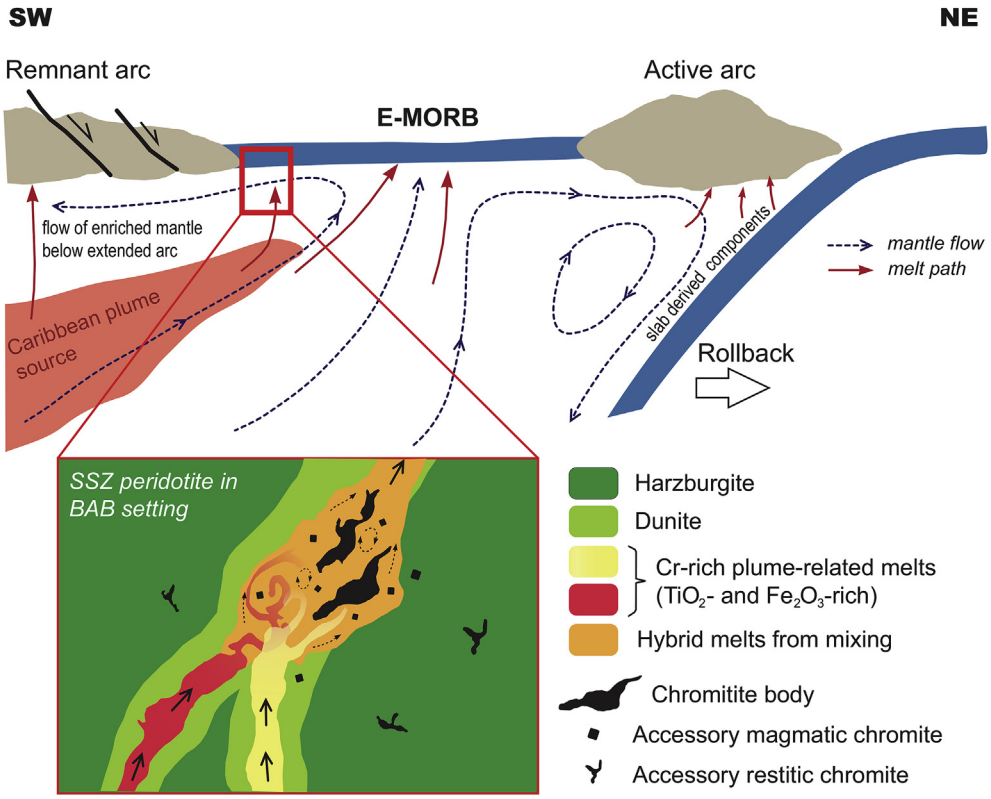


**Fig. 12.** Schematic tectonomagmatic model for the formation of chromitites from the northern and central parts of the Loma Caribe peridotite during the Late Cretaceous. The mantle flow convective regime beneath the back-arc basin is based on Gribble et al. (1998) and Taylor and Martínez (2003). After the extension of the volcanic arc and the development of an intra-arc/back-arc basin, the Loma Caribe peridotite, originally formed at a fore-arc setting, was emplaced at the back-arc mantle. The deeper Caribbean-plume enriched source is incorporated by lateral flow from the SW, giving place to enriched plume-related magmatism similar to E-MORB. Cr-rich plume-related melts with different $SiO_2$ content (red and yellow) infiltrate Loma Caribe peridotite through pre-existing dunites. The melts meet at the intersection of dunite channels and mix producing hybrid melts able to precipitate volumes of chromitite. Accessory magmatic chromite, with subhedral shape, crystallizes from these melts in the host peridotite. Accessory restitic chromite, with vermicular shape, was already present in the peridotites.

and Kelemen, 2002; González-Jiménez et al., 2014b, and references therein). Melts infiltrated through these dunite pathways by porous flow in a melt-film network (O'Reilly and Griffin, 2012) along contacts between silicates, until they produced focused porous flow melt. The melt-filled dunite channels intersected and contributed to the mixing of melts of different provenances or with different degrees of fractionation to generate hybrid melts (González-Jiménez et al., 2014b). The mixing of variably differentiated (more or less $SiO_2$-rich) basaltic melts within dunitic melt flow channels caused the saturation in chromian spinel, producing monomineralic concentrations of chromite (e.g., Irvine, 1977; Arai and Yurimoto, 1994; Zhou et al., 1996, 1998; Ballhaus, 1998).

## 6. Conclusions

Chromitites from the northern and central parts of the Loma Caribe peridotite are hosted in the mantle section of a supra-subduction zone (SSZ) ophiolite. However, their chemical composition, with high concentrations in $Cr_2O_3$, $TiO_2$, $Fe_2O_3$ and PGE (with a consistent positive Pt anomaly) and relatively enrichment in Ga, V, Co, Mn, and Zn, strongly differs from that of other mantle-hosted chromitites. This anomalous composition results from the interaction of a mantle plume with a back-arc mantle. The intrusive character of the chromitites is also revealed by the presence of two texturally and chemically distinct types of accessory chromite in the host peridotite, one related to the chromitite-forming magmas and the other corresponding to restitic chromite from a MOR or an abyssal peridotite. The northern and central chromitites of the Loma Caribe peridotite are the first reported example of chromitite resulting from the interaction of a mantle plume with a supra-subduction mantle in a back-arc basin setting. Moreover, the proposed model is the first attempt to enlighten the effect that mantle plumes may have on the genesis of mantle hosted chromitites.

## Declaration of competing interest

The authors declare that they have no known competing financial interests or personal relationships that could have appeared to influence the work reported in this paper.

## Acknowledgements

Funding for this research was provided by the *Fondo Europeo de Desarrollo Regional* (FEDER) Funds, the Spanish Project CGL2015-65824 granted by the Spanish *Ministerio de Economía y Competitividad* (MINECO) to JAP and RTI2018-099157-A-I00 *Ministerio de Ciencia, Innovación y Universidades* (MICINN) to JMGJ. Additional funding was obtained from the Ramón y Cajal Fellowship RYC-2015-17596 to JMGJ (sponsored by MICINN), the Ph.D. grant BES-2016-076887 to JFdP (sponsored by MINECO), and the Mexican research programs *Ciencia Básica* (A1-S-14574) sponsored by the *Consejo Nacional de Ciencia y Tecnología* (CONACYT) from Mexico, and the *Programa de Apoyo a Proyectos de Investigación e Innovación tecnológica* (IA-101419) sponsored by the UNAM. Additional support was provided by the University of Barcelona and University of Granada, Spain. We also thank Dr. Carlos Ortega-Obregón (*Laboratorio de Estudios Isotópicos of Centro de Geociencias*, UNAM, Mexico) for the help with the Laser ICP-MS analyses on chromite.

## Appendix A. Supplementary data

Supplementary data to this article can be found online at https://doi.org/10.1016/j.gsf.2020.05.005.

## References

Ahmed, A., Arai, S., 2002. Unexpectedly high-PGE chromitite from the deeper mantle section of the northern Oman ophiolite and its tectonic implications. Contrib. Mineral. Petrol. 143, 263–278.

Aiglsperger, T., Proenza, J.A., Zaccarini, F., Lewis, J.F., Garuti, G., Labrador, M., Longo, F., 2015. Platinum group minerals (PGM) in the Falcondo Ni-laterite deposit, loma Caribe peridotite (Dominican Republic). Miner. Deposita 50, 105–123.

Amossé, J., Dable, P., Allibert, M., 2000. Thermochemical behavior of Pt, Ir, Rh and Ru vs. $fO_2$ and $fS_2$ in a basaltic melt. Implications for the differentiation and precipitation of these elements. Mineral. Petrol. 68, 9–62.

Anenburg, M., Mavrogenes, J.A., 2016. Experimental observation on noble metal nanonuggets and Fe-Ti oxides, and the transport of platinum group elements in silicate melts. Geochem. Cosmochim. Acta 192, 258–278.

Arai, S., 2013. Conversion of low-pressure chromitites to ultrahigh-pressure chromitites by deep recycling: a good inference. Earth Planet Sci. Lett. 379, 81–87.

Arai, S., Abe, N., 1995. Reaction of orthopyroxene in peridotite xenoliths with alkali-basalt melt and its implication for genesis of Alpine-type chromitite. Am. Mineral. 80, 1041–1047.

Arai, S., Miura, M., 2016. Formation and modification of chromitites in the mantle. Lithos 264, 277–295.

Arai, S., Yurimoto, H., 1994. Podiform chromitites from the Tari-Misaka ultramafic complex, southwestern Japan, as a melt mantle interaction products. Econ. Geol. 89, 1279–1288.

Aulbach, S., Mungall, J.E., Pearson, D.G., 2016. Distribution and processing of highly siderophile elements in cratonic mantle lithosphere. Rev. Mineral. Geochem. 81, 239–304.

Ballhaus, C., 1998. Origin of podiform chromite deposits by magma mingling. Earth Planet Sci. Lett. 156, 185–193.

Ballhaus, C., Bockrath, C., Wohlgemuth-Ueberwasser, C., Laurenz, V., Berndt, J., 2006. Fractionation of noble metals by physical processes. Contrib. Mineral. Petrol. 152, 667–684.

Ballhaus, C., Wirth, R., Fonseca, R.O.C., Blanchard, H., Pröll, W., Bragagni, A., Nagel, T., Schreiber, A., Dittrich, S., Thome, V., Hezel, D.C., Below, R., Cieszynski, H., 2017. Ultra-high pressure and ultra-reduced minerals in ophiolites may form by lightning strikes. Geochem. Perspect. Lett. 5, 42–46.

Barnes, S.J., Roeder, P.L., 2001. The range of spinel compositions in terrestrial mafic and ultramafic rocks. J. Petrol. 42, 2279–2302.

Bockrath, C., Ballhaus, C., Holzheid, A., 2004. Fractionation of the platinum-group elements during mantle melting. Science 305, 1951–1953.

Bonavia, F.F., Diella, V., Ferrario, A., 1993. Precambrian podiform chromitites from Kenticha Hill, southern Ethiopia. Econ. Geol. 88, 198–202.

Borisov, A., Palme, H., 2000. Solubilities of noble metals in Fe containing melts as derived from experiments in Fe-free systems. Am. Mineral. 85, 1665–1673.

Braun, M.G., Kelemen, P.B., 2002. Dunite distribution in the Oman Ophiolite: implications for melt flux through porous dunite conduits. G-cubed 3 (11), 8603. https://doi.org/10.1029/2001GC000289.

Cabri, L.J., 2002. The platinum-group minerals. In: Cabri, L.J. (Ed.), The Geology, Geochemistry, Mineralogy and Mineral Beneficiation of Platinum-Group Elements, Canadian Institute of Mining Metallogeny and Petroleum, Special Volume, vol. 54, pp. 13–130.

Campbell, I.H., 2001. Identification of ancient mantle plumes. In: Ernst, R.E., Buchan, K.L. (Eds.), Mantle Plumes: Their Identification through Time. GSA Am. Spec. Pap., vol. 352, pp. 5–21.

Campbell, I.H., Griffiths, R.W., 1990. Implications of mantle plume structure for the evolution of flood basalts. Earth Planet Sci. Lett. 99, 79–93.

Colás, V., González-Jiménez, J.M., Griffin, W.L., Fanlo, I., Gervilla, F., O'Reilly, S.Y., Pearson, N.J., Kerestedjian, T., Proenza, J.A., 2014. Fingerprints of metamorphism in chromite: new insights from minor and trace elements. Chem. Geol. 389, 137–152.

Colás, V., González-Jiménez, J.M., Camprubí, A., Proenza, J.A., Griffin, W.L., Fanlo, I., O'Reilly, S.Y., Gervilla, F., González-Partida, E., 2019. A reappraisal of the metamorphic history of the Tehuitzingo chromitite, Puebla state, Mexico. Int. Geol. Rev. 61 (14), 1706–1727. https://doi.org/10.1080/00206814.2018.1542633.

Cottrell, E., Walker, D., 2006. Constraints on core formation from Pt partitioning in mafic silicate liquids at high temperatures. Geochem. Cosmochim. Acta 70, 1565–1580.

Dare, S.A.S., Pearce, J.A., McDonald, I., Styles, M.T., 2009. Tectonic discrimination of peridotites using $fO_2$–Cr# and Ga–Ti–Fe III systematics in chrome-spinel. Chem. Geol. 261, 199–216.

Derbyshire, E.J., O'Driscoll, B., Lenaz, D., Zanetti, A., Gertisser, R., 2019. Chromitite petrogenesis in the mantle section of the Ballantrae ophiolite complex (Scotland). Lithos 344–345, 51–67.

Dick, H.J., Bullen, T., 1984. Chromian spinel as a petrogenetic indicator in abyssal and alpine-type peridotites and spatially associated lavas. Contrib. Mineral. Petrol. 86, 54–76.

Donnelly, T.W., Beets, D., Carr, M.J., Jackson, T., Klaver, G., Lewis, J., Maury, R., Schellenkens, H., Smith, A.L., Wadge, G., Westercamp, D., 1990. History and tectonic setting of Caribbean magmatism. In: Dengo, G., Case, J. (Eds.), The Caribbean Region. The Geology of North America. Geological Society of America, Vol. H, pp. 339–374.

Draper, G., Gutiérrez, G., Lewis, J.F., 1996. Thrust emplacement of the Hispaniola peridotite belt: orogenic expression of the mid-Cretaceous Caribbean arc polarity reversal? Geology 24, 1143–1146.

Draper, G., Lewis, J.F., 1991. Metamorphic belts in central Hispaniola. In: Mann, P., Draper, G., Lewis, J.F. (Eds.), Geologic and Tectonic Development of the North America-Caribbean Plate Boundary in Española, vol. 262. Geological Society of America Special Paper, pp. 29–46.

Draper, G., Mann, P., Lewis, J.F., 1994. Hispaniola. In: Donovan, S.K., Jackson, T.A. (Eds.), Caribbean Geology: an Introduction. Kingston, Jamaica. University of the West Indies Publishers Association, pp. 129–150.

Draper, G., Nagle, F., 1991. Geology, structure, and tectonic development of the Río san juan complex, northern Dominican Republic. In: Mann, P., Draper, G., Lewis, J.F. (Eds.), Geologic and Tectonic Development of the North America-Caribbean Plate Boundary in Hispaniola, vol. 262. Geological Society of America Special Paper, pp. 77–95.

Economou, M., 1983. Platinum group metals in chromite ores from the Vourinos Ophiolite Complex. Greece. Ofioliti 8, 339–356.

Economou-Eliopoulos, M., 2010. Platinum-group elements (PGE) in various geotectonic settings: opportunities and risks. Hellenic J. Geosci. 45, 65–82.

Eliopoulos, I.P.D., Eliopoulos, G.D., 2019. Factors controlling the gallium preference in high-Al chromitites. Minerals 9, 623.

Ely, J.C., Neal, C.R., 2003. Using platinum-group elements to investigate the origin of the Ontong Java Plateau, SW Pacific. Chem. Geol. 196, 235–257.

Ernst, R.E., Buchan, K.L., 2003. Recognizing mantle plumes in the geological record. Annu. Rev. Earth Planet Sci. 31, 469–523.

Escuder-Viruete, J., Castillo-Carrión, M., Pérez-Estaún, A., 2014. Magmatic relationships between depleted mantle harzburgites, boninitic cumulate gabbros and subduction-

related tholeiitic basalts in the Puerto Plata ophiolitic complex, Dominican Republic: implications for the birth of the Caribbean island-arc. Lithos 196–197, 261–280.
Escuder-Viruete, J., Contreras, F., Stein, G., Urien, P., Joubert, M., Pérez-Estaún, A., Friedman, R., Ullrich, T., 2007b. Magmatic relationships and ages between adakites, magnesian andesites and Nb-enriched basalt-andesites from Hispaniola: record of a major change in the Caribbean island arc magma sources. Lithos 99, 151–177.
Escuder-Viruete, J., Díaz-De-Neira, A., Hernáiz-Huerta, P.P., Monthel, J., García-Senz, J., Joubert, M., Lopera, E., Ullrich, T., Friedman, R., Mortensen, J., Pérez-Estaún, A., 2006. Magmatic relationships and ages of Caribbean Island arc tholeiites, boninites and related felsic rocks, Dominican Republic. Lithos 90, 161–186.
Escuder-Viruete, J., Friedman, R., Castillo-Carrión, M., Jabites, J., Pérez-Estaún, A., 2011a. Origin and significance of the ophiolite high-P mélanges in the northern Caribbean convergent margin: insights from the geochemistry and large-scale structure of the Río San Juan metamorphic complex. Lithos 127 (3), 483–504.
Escuder-Viruete, J., Hernaiz, P.P., Draper, G., Gutiérrez-Alonso, G., Lewis, J.F., Pérez-Estaún, A., 2002. El metamorfismo de la Formacion Maimón y los Complejos Duarte y Río Verde, Cordillera Central Dominicana: implicaciones en la estructura y la evolucion del primitivo arco isla caribeño. Acta Geol. Hisp. 37 (2–3), 123–162 (in Spanish).
Escuder-Viruete, J., Joubert, M., Abad, M., Pérez-Valera, F., Gabites, J., 2016. The basaltic volcanism of the Dumisseau formation in the Sierra de Bahoruco, SW Dominican Republic: a record of the mantle plume-related magmatism of the caribbean large igneous province. Lithos 254–255, 67–83. https://doi.org/10.1016/j.lithos.2016.03.013.
Escuder-Viruete, J., Joubert, M., Urien, P., Friedman, R., Weis, D., Ullrich, T., Pérez-Estaún, A., 2008. Caribbean island-arc rifting and back-arc basin development in the Late Cretaceous: geochemical, isotopic and geochronological evidence from Central Hispaniola. Lithos 104, 378–404.
Escuder-Viruete, J., Pérez-Estaún, A., Contreras, F., Joubert, M., Weis, D., Ullrich, T.D., Spadea, P., 2007a. Plume mantle source heterogeneity through time: insights from the Duarte Complex, Hispaniola, northeastern Caribbean. J. Geophys. Res. 112, B04203.
Escuder-Viruete, J., Pérez-Estaún, A., Weis, D., 2009. Geochemical constraints on the origin of the late Jurassic proto-Caribbean oceanic crust in Hispaniola. Int. J. Earth Sci. 98 (2), 407–425.
Escuder-Viruete, J., Pérez-Estaún, A., Weis, D., Friedman, R., 2010. Geochemical characteristics of the Río Verde complex, central Hispaniola: implications for the paleotectonic reconstruction of the lower Cretaceous Caribbean island-arc. Lithos 114, 168–185.
Escuder-Viruete, J., Pérez-Estaún, A., Joubert, M., Weis, D., 2011b. The Pelona-Pico Duarte basalts formation, central Hispaniola: an on-land section of late Cretaceous volcanism related to the Caribbean large igneous province. Geol. Acta 9, 307–328.
Escuder-Viruete, J., Pérez-Estaún, A., Gabites, J., Suárez-Rodríguez, A., 2011c. Structural development of a high-pressure collisional accretionary wedge: the Samaná complex, northern Hispaniola. J. Struct. Geol. 33 (5), 928–950.
Fellows, S.A., Canil, D., 2012. Experimental study of the partitioning of Cu during partial melting of Earth's mantle. Earth Planet Sci. Lett. 337, 133–143.
Farré-de-Pablo, J., Proenza, J.A., González-Jiménez, J.M., Garcia-Casco, A., Colás, V., Roqué-Rosell, J., Camprubí, A., Sánchez-Navas, A., 2018. A shallow origin for diamonds in ophiolitic chromitites. Geology 47, 75–78.
Finnigan, C.S., Brenan, J.M., Mungall, J.E., McDonough, W.F., 2008. Experiments and models bearing on the role of chromite as a collector of platinum group minerals by local reduction. J. Petrol. 49 (9), 1647–1665.
Gale, A., Dalton, C.A., Langmuir, C.H., Su, Y., Schilling, J.G., 2013. The mean composition of ocean ridge basalts. G-cubed 14, 489–518.
Garuti, G., Fershtater, G., Bea, F., Montero, P., Pushkarev, E.V., Zaccarini, F., 1997. Platinum-group elements as petrological indicators in mafic–ultramafic complexes of the central and southern Urals: preliminary results. Tectonophysics 276, 181–194.
Garuti, G., Pushkarev, E., Zaccarini, F., Cabella, R., Anikina, E., 2003. Chromite composition and platinum-group mineral assemblage in the Uktus Uralian-Alaskan-type complex (Central Urals, Russia). Miner. Deposita 38, 312–326.
Gervilla, F., Proenza, J.A., Frei, R., González-Jiménez, J.M., Garrido, C.J., Melgarejo, J.C., Meibom, A., Díaz-Martínez, R., Lavaut, W., 2005. Distribution of platinum-group elements and Os isotopes in chromite ores from Mayarí-Baracoa Ophiolitic Belt (eastern Cuba). Contrib. Mineral. Petrol. 150, 589–607.
Gómez Sainz de Aja, J.A., 1999. Mapa Geológico de la Hoja a E. 1:50.000 nº 6172-IV (Bonao). Proyecto SYSMIN de Cartografía Geotemática de la República Dominicana. Dirección General de Minería, Santo Domingo (in Spanish).
González-Jiménez, J.M., Griffin, W.L., Gervilla, F., Proenza, J.A., O'Reilly, S.Y., Pearson, N.J., 2014a. Chromitites in ophiolites: how, where, when, why? Part I. A review and new ideas on the origin and significance of platinum-group minerals. Lithos 189, 127–139.
González-Jiménez, J.M., Griffin, W.L., Proenza, J.A., Gervilla, F., O'Reilly, S.Y., Akbulut, M., Pearson, N.J., Arai, S., 2014b. Chromitites in ophiolites: how, where, when, why? Part II. The crystallization of chromitites. Lithos 189, 140–158.
González-Jiménez, J.M., Locmelis, M., Belousova, E., Griffin, W.L., Gervilla, F., Kerestedjian, T.M., O'Reilly, S.Y., Pearson, N.J., Sergeeva, I., 2015. Genesis and tectonic implications of podiform chromitites in the metamorphosed ultramafic massif of Dobromirtsi (Bulgaria). Gondwana Res. 27, 555–574.
González-Jiménez, J.M., Proenza, J.A., Gervilla, F., Melgarejo, J.C., Blanco-Moreno, J.A., Ruiz-Sánchez, R., Griffin, W.L., 2011. High-Cr and high-Al chromitites from Sagua de Tánamo district, Mayarí-Cristal ophiolitic massif (eastern Cuba): constraints on their origin from mineralogy and geochemistry of chromian spinel and platinum-group elements. Lithos 125, 101–121.
Graham, I.T., Franklin, B.J., Marshall, B., 1996. Chemistry and mineralogy of podiform chromitite deposits, southern NSW, Australia: a guide to their origin and evolution. Mineral. Petrol. 57, 129–150.
Gribble, R.F., Stern, R.J., Newman, S., Bloomer, S.H., O'Hearn, T., 1998. Chemical and isotopic composition of lavas from the northern Mariana Trough: implications for magma genesis in back-arc basins. J. Petrol. 39, 125–154.
Griffin, W.L., Afonso, J.C., Belousova, E.A., Gain, S.E., Gong, X.H., González-Jiménez, J.M., Howell, D., Huang, J.X., McGowan, N., Pearson, N.J., Satsukawa, T., Shi, R., Williams, P., Xiong, Q., Yang, J.S., Zhang, M., O'Reilly, S.Y., 2016. Mantle recycling: transition zone metamorphism of Tibetan ophiolitic peridotites and its tectonic implications. J. Petrol. 57, 655–684.
Griffin, W.L., Howell, D., González-Jiménez, J.M., Xiong, Q., O'Reilly, S.Y., 2018. Comment on "Ultra-high pressure and ultra-reduced minerals in ophiolites may form by lightning strikes". Geochem. Perspect. Lett. 7, 1–2.
Haldemann, E.G., Buchan, R., Blowes, V.H., Chandler, T., 1979. Geology of the laterite nickel deposits, Dominican Republic. In: Evans, D.J., Shoemaker, R.S., Velman, H. (Eds.), International Laterite Symposium. Society of Mining Engineers, New Orleans, Louisiana, pp. 57–84.
Hastie, A.R., Kerr, A.C., Mitchell, S.F., Millar, I.L., 2008. Geochemistry and petrogenesis of Cretaceous oceanic plateau lavas in eastern Jamaica. Lithos 101, 323–343.
Hernaiz Huerta, P.P., Lewis, J.F., Escuder-Viruete, J., Gutiérrez, G., Mortensen, J., Hames, W., Solé, J., Martínez, A., Draper, G., 2000. Memoria explicativa del Mapa Geológico a escala 1:50.000 de Villa Altagracia (6172-II). Proyecto de Cartografía Geotemática de la República Dominicana. Dirección General de Minería, Santo Domingo (in Spanish).
Helmy, H.M., Ballhaus, C., Wohlgemuth-Ueberwasser, C., Fonseca, R.O.C., Laurenz, V., 2010. Partitioning of Se, As, Sb, Te and Bi between monosulfide solid solution and sulfide melt – application to magmatic sulfide deposits. Geochem. Cosmochim. Acta 74, 6174–6179.
Henares, S., González-Jiménez, J.M., Gervilla, F., Proenza, J.A., Rodríguez, A.C., González-Pontón, R.B., 2010. Las cromititas del complejo ofiolítico de Camagüey, Cuba: un ejemplo de cromitas ricas en Al. Bol. Soc. Geol. Mex. 62, 173–185 (in Spanish).
Hicky, R.L., Frey, F.A., 1982. Geochemical characteristics of boninite series volcanic: implication for their source. Geochem. Cosmochim. Acta 46, 2099–2115.
Irvine, T.N., 1977. Origin of chromitite in the Muskov intrusion and other stratiform intrusions: a new interpretation. Geology 5, 273–277.
Ismail, S.A., Mirza, T., Carr, P., 2010. Platinum-group elements geochemistry in podiform chromitites and associated peridotites of the Mawat ophiolite, northeastern Iraq. J. Asian Earth Sci. 37, 31–41.
Kamenetsky, V.S., Crawford, A.J., Meffre, S., 2001. Factors controlling chemistry of magmatic spinel: an empirical study of associated olivine, Cr-spinel and melt inclusions from primitive rocks. J. Petrol. 42, 655–671.
Kelemen, P.B., Hanghoj, K., Greene, A.R., 2004. One view of the geochemistry of subduction-related magmatic arcs, with an emphasis on primitive andesite and lower crust. In: Holland, H.D., Turekian, K.K. (Eds.), Treatise on Geochemistry, vol. 3. Elsevier, Amsterdam, pp. 593–659.
Kerr, A.C., Tarney, J., Marriner, G.F., Nivia, A., Saunders, A.D., 1997. The Caribbean–Colombian Cretaceous igneous province: the internal anatomy of an oceanic plateau. In: Mahoney, J., Coffin, M.F. (Eds.), Large-igneous Provinces. AGU, Washington DC, pp. 123–144.
Kesler, S.E., Campbell, I.H., Allen, C.M., 2005. Age of the Los Ranchos Formation, Dominican Republic: timing and tectonic setting of primitive island arc volcanism in the Caribbean region. Geol. Soc. Am. Bull. 117, 987–995.
König, S., Luguet, A., Lorand, J.-P., Wombacher, F., Lissner, M., 2012. Selenium and tellurium systematics of the Earth's mantle from high precision analyses of ultra-depleted orogenic peridotites. Geochem. Cosmochim. Acta 86, 354–366.
Krebs, M., Maresch, W.V., Schertl, H.-P., Baumann, A., Draper, G., Idleman, B., Münker, C., Trapp, E., 2008. The dynamics of intra-oceanic subduction zones: a direct comparison between fossil petrological evidence (Rio San Juan Complex, Dominican Republic) and numerical simulation. Lithos 103, 106–137. https://doi.org/10.1016/j.lithos.2007.09.003.
Krebs, M., Shertl, H.P., Maresch, W.V., Draper, G., 2011. Mass flow in serpentinite-hosted subduction channels: P-T-t path patter of metamorphic blocks in the Rio San Juan mélange (Dominican Republic). J. Asian Earth Sci. 42, 569–595.
Lapierre, H., Bosch, D., Dupuis, V., Polvé, M., Maury, R., Hernandez, J., Monié, P., Yeghicheyan, D., Jaillard, E., Tardy, M., de Lepinay, B., Mamberti, M., Desmet, A., Keller, F., Senebier, F., 2000. Multiple plume events in the genesis of the peri-Caribbean Cretaceous oceanic plateau province. J. Geophys. Res. 105, 8403–8421.
Lapierre, H., Dupuis, V., Lepinay, B.M., Tardy, M., Ruiz, J., Maury, R.C., Hernandez, J., Loubert, M., 1997. Is the lower Duarte complex (Hispaniola) a remnant of the caribbean plume generated oceanic plateau? J. Geol. 105, 111–120.
Lapierre, H., Dupuis, V., de Lepinay, B.M., Bosch, D., Monié, P., Tardy, M., Maury, R.C., Hernández, J., Polvé, M., Yeghicheyan, D., Cotton, J., 1999. Late Jurassic oceanic crust and upper Cretaceous Caribbean plateau picritic basalts exposed in the Duarte igneous complex, Hispaniola. J. Geol. 107, 193–207.
Leblanc, M., 1991. Platinum-group elements and gold in ophiolitic complexes: distribution and fractionation from mantle to oceanic floor. In: Peters, T.J., Nicolas, A., Coleman, R.G. (Eds.), Ophiolite Genesis and Evolution of Oceanic Lithosphere. Kluwer Academic Publ., Dordrecht, The Netherlands, pp. 231–260.
Leblanc, M., Nicolas, A., 1992. Les chromitites ophiolitiques. Chron. Rech. Min. 507, 3–25 (in French).
Leblanc, M., Violette, J.F., 1983. Distribution of aluminum-rich and chromium-rich chromite pods in ophiolite peridotites. Econ. Geol. 78, 293–301.

Lenaz, D., Kamenetsky, V.S., Crawford, A.J., Princivalle, F., 2000. Melt inclusions in detrital spinels from the SE Alps (Italy–Slovenia): a new approach to provenance studies of sedimentary basins. Contrib. Mineral. Petrol. 139, 748–758.
Lewis, J.F., Astacio, V.A., Espaillat, J., Jiménez, J., 2000. The occurrence of volcanogenic massive sulfide deposits in the maimon formation, Dominican Republic: the cerro de Maimón, loma pesada and loma barbuito deposits. In: Sherlock, R., Barsch, R., Logan, A. (Eds.), VMS Deposits of Latin America. Geological Society of Canada Special Publication, pp. 223–249.
Lewis, J.F., Escuder-Viruete, J., Hernaiz Huerta, P.P., Gutiérrez, J., Draper, G., Pérez-Estaún, A., 2002. Geochemical subdivision of the Circum-Caribbean Island Arc, Dominican Cordillera Central: implications for crustal formation, accretion and growth within an intra-oceanic setting. Acta Geol. Hisp. 37, 81–122.
Lewis, J.F., Draper, G., 1990. Geology and tectonic evolution of the Northern Caribbean margin. In: Dengo, G., Case, J.E. (Eds.), The Geology of North America, Vol. H, the Caribbean Region. The Geological Society of America, pp. 77–140.
Lewis, J.F., Draper, G., Proenza, J.A., Espaillat, J., Jiménez, J., 2006. Ophiolite-related ultramafic rocks (serpentinites) in the Caribbean region: a review of their occurrence, composition, origin, emplacement and Ni-laterite soil formation. Geol. Acta 4 (1–2), 237–263.
Lewis, J.F., Jimenez, G.J.G., 1991. Duarte Complex in the La Vega – Jarabacoa – Janico area, central Hispaniola; geological and geochemical features of the sea floor during early stages of arc evolution. In: Mann, P., Draper, G., Lewis, J.F. (Eds.), Geologic and Tectonic Development of North America – Caribbean Plate Boundary in Hispaniola, vol. 262. Geological Society of America Special Paper, pp. 115–141.
Loewen, M.W., Duncan, R.A., Kent, A.J.R., Krawl, K., 2013. Prolonged plume volcanism in the Caribbean large igneous province: new insights from Curaçao and Haiti. G-cubed 14, 4241–4259. https://doi.org/10.1002/ggge.20273.
Lorand, J.P., Grégoire, M., 2006. Petrogenesis of base metal sulfides of some peridotites of the Kaapvaal craton (South Africa). Contrib. Mineral. Petrol. 151, 521–538.
Luguet, A., Lorand, J.P., Seyler, M., 2003. Sulfide petrology and highly siderophile element geochemistry of abyssal peridotites: a coupled study of samples from the Kane Fracture Zone (45°W 23°20′N, MARK Area, Atlantic Ocean). Geochem. Cosmochim. Acta 71, 3082–3097.
Luguet, A., Reisberg, L., 2016. Highly siderophile element and $^{187}Os$ signatures in non-cratonic basalt-hosted peridotite xenoliths: unravelling the origin and evolution of the post-archean lithospheric mantle. Rev. Mineral. Geochem. 81, 305–367.
Mann, P., Calais, E., Ruegg, J.C., De Mets, C., Jansma, P., Mattioli, G., 2002. Oblique collision in the northeastern Caribbean from GPS measurements and geological observations. Tectonics 21 (6), 1–26.
Mann, P., Draper, G., Lewis, J.F., 1991. An overview of the geologic and tectonic development of Hispaniola. In: Mann, P., Draper, G., Lewis, J.F. (Eds.), Geologic and Tectonic Development of the North America – Caribbean Plate Boundary in Hispaniola. Geological Society of America Special, Boulder, Colorado. Paper 262.
Marchesi, C., Garrido, C.J., Proenza, J.A., Hidas, K., Varas-Reus, M.I., Butjosa, L., Lewis, J.F., 2016. Geochemical record of subduction initiation in the sub-arc mantle: insights from the Loma Caribe peridotite (Dominican Republic). Lithos 252–253, 1–15.
Martínez, F., Taylor, B., 2002. Mantle wedge control on back-arc crustal accretion. Nature 416, 417–420.
Mathez, E.A., Kinzler, R.J., 2017. Metasomatic chromitite seams in the Bushveld and Rum layered intrusions. Elements 13, 397–402.
Matsumoto, I., Arai, S., 2001. Morphological and chemical variations of chromian spinel in dunite-harzburgite complexes from the Sangun zone (SW Japan): implications for mantle/melt reaction and chromitite formation processes. Mineral. Petrol. 73, 305–323.
Maurel, C., 1984. Étude expérimentale de l'équilibre spinelle chromifère-liquide silicaté basique. Société Française de Minéralogie et cristallographie Congrès "Les Spinelles" (in French).
Mavrogenes, J.A., O'Neill, H.StC., 1999. The relative effects of pressure, temperature, and oxygen fugacity on the solubility of sulfide in mafic magmas. Geochem. Cosmochim. Acta 63, 1173–1180.
McGowan, N.M., Griffin, W.L., González-Jiménez, J.M., Belousova, E.A., Afonso, J., Shi, R., McCammon, C.A., Pearson, N.J., O'Reilly, S.Y., 2015. Tibetan chromitites: excavating the slab graveyard. Geology 43, 179–182.
Médar, E., Schmidt, M.W., Wälle, M., Keller, N.S., Günther, D., 2015. Platinum partitioning between metal and silicate melts: core formation, late veneer and the nanonuggets issue. Geochem. Cosmochim. Acta 162, 183–201.
Melcher, F., Grum, W., Thalhammer, T.V., Thalhammer, O.A.R., 1999. The giant chromite deposits at Kempirsai, Urals: constraints from trace element (PGE, REE) and isotope data. Miner. Deposita 34, 250–272.
Melcher, F., Grum, W., Simon, G., Thalhammer, T.V., Stumpfl, E.F., 1997. Petrogenesis of the ophiolitic giant chromite deposits of Kempirsai, Kazakhstan: a study of solid and fluid inclusions in chromite. J. Petrol. 38, 1419–1458.
Miura, M., Arai, S., Ahmed, A.H., Mizukami, M., Okuno, M., Yamamoto, S., 2012. Podiform chromitite classification revisited: a comparison of discordant and concordant chromitite pods from Wadi Hilti, northern Oman ophiolite. J. Asian Earth Sci. 59, 52–61.
Moussallam, Y., Longpré, M.A., McCammon, C., Gomez-Ulla, A., Rose-Koga, E.F., Scaillet, B., Peters, N., Gennaro, E., Paris, R., Oppenheimer, C., 2019. Mantle plumes are oxidised. Earth Planet Sci. Lett. 527, 115798.
Mukherjee, R., Mondal, S.K., Rosing, M.T., Frei, R., 2010. Compositional variations in the Mesoarchean chromites of the Nuggihalli schist belt, Western Dharwar craton (India): potential parental melts and implications for tectonic setting. Contrib. Mineral. Petrol. 160, 865–885.
Mungall, J.E., 2005. Magmatic geochemistry of the platinum-group elements. In: Mungall, J.E. (Ed.), Exploration for Platinum-Group Elements Deposits. Short Course Ser Vol 35. Mineral Assoc Canada, pp. 1–34.
Naldrett, A.J., Duke, J.M., 1980. Pt metals in magmatic sulphide ores. Sciences 208, 1417–1424.
O'Driscoll, B., González-Jiménez, J.M., 2016. Petrogenesis of the platinum-group minerals. Rev. Mineral. Geochem. 81, 4889–5578.
O'Reilly, S.Y., Griffin, W.L., 2012. Mantle metasomatism. In: Harlov, D.E., Austrheim, H. (Eds.), Metasomatism and the Chemical Transformation of Rock, Lecture Notes in Earth System Sciences. Springer-Verlag Berlin, Heidelberg, pp. 467–528.
Pagé, P., Barnes, S.J., 2009. Using trace elements in chromites to constrain the origin of podiform chromitites in the Thetford Mines ophiolite, Quebec, Canada. Econ. Geol. 104, 997–1018.
Pedersen, R.-B., Johannesen, G.M., Boyd, R., 1993. Stratiform platinum-group element mineralizations in the ultramafic cumulates of the Leka ophiolite complex, central Norway. Econ. Geol. 88, 782–803.
Pérez-Estaún, A., Hernaiz Huerta, P.P., Lopera, E., Joubert, M., Escuder-Viruete, J., Díaz de Neira, A., Monthel, J., García-Senz, Ubrien, P., Contreras, F., Bernárdez, F., Stein, G., Deschamps, I., García-Lobón, J.L., Ayala, C., 2007. Geología de la República Dominicana: de la construcción de arco-isla a la colisión arco-continente. Bol. Geol. Min. 118 (2), 157–174 (in Spanish).
Pindell, J.L., Kennan, L., 2009. Tectonic evolution of the Gulf of Mexico, Caribbean and northern South America in the mantle reference frame: an update. Geological Soc. London Special Publ. 328 (1), 1–55.
Pindell, J.L., Maresch, W.V., Martens, U., Stanek, K., 2012. The Greater Antillean Arc: early Cretaceous origin and proposed relationship to Central American subduction mélanges: implications for models of Caribbean evolution. Int. Geol. Rev. 54, 131–143.
Prichard, H.M., Neary, C.R., Fisher, P.C., O'Hara, M.J., 2008. PGE-rich podiform chromitites in the Al'Ays ophiolites complex, Saudi Arabia: an example of critical mantle melting to extract and concentrate PGE. Econ. Geol. 103, 1507–1529.
Proenza, J., Gervilla, F., Melgarejo, J.C., Bodinier, J.L., 1999. Al- and Cr- rich chromitites from the Mayarí–Baracoa ophiolitic belt (eastern Cuba): consequence of interaction between volatile-rich melts and peridotites in suprasubduction mantle. Econ. Geol. 94, 547–566.
Proenza, J.A., Zaccarini, F., Lewis, J.F., Longo, F., Garuti, G., 2007. Chromian spinel composition and the platinum-group minerals of the PGE-rich Loma Peguera chromitites, Loma Caribe peridotite, Dominican Republic. Can. Mineral. 45, 631–648.
Pujol-Solà, N., Proenza, J.A., Garcia-Casco, A., González-Jiménez, J.M., Andreazini, A., Melgarejo, J.C., Gervilla, F., 2018. An alternative scenario on the origin of ultra-high pressure (UHP) and super-reduced (SuR) minerals in ophiolitic chromitites: a case study from the Mercedita Deposit (Eastern Cuba). Minerals 8, 433.
Révillon, S., Hallot, E., Arndt, N., Chauvel, C., Duncan, R.A., 2000. A complex history for the caribbean plateau: petrology, geochemistry, and geochronology of the beata ridge, south Hispaniola. J. Geol. 108, 641–661.
Richards, M.A., Duncan, R.A., Courtillot, V.E., 1989. Flood basalts and hot-Spot tracks: plume heads and tails. Science 246, 103–107.
Robinson, P.T., Trumbull, R.B., Schmitt, A., Yang, J.S., Li, J.W., Zhou, M.F., Erzinger, J., Dare, S., Xiong, F., 2015. The origin and significance of crustal minerals in ophiolitic chromitites and peridotites. Gondwana Res. 27, 486–506.
Robinson, P.T., Zhou, M.F., Malpas, J., Bai, W.J., 1997. Podiform chromitites: their composition, origin and environment of formation. Episodes 20, 247–252.
Rollinson, H., 2008. The geochemistry of mantle chromitites from the northern part of the Oman ophiolite: inferred parental melt compositions. Contrib. Mineral. Petrol. 156, 273–288.
Rollinson, H., 2016. Surprises from the top of the mantle transition zone. Geol. Today 32 (2), 58–64.
Rollinson, H., Reid, C., Windley, B., 2010. Chromitites from the Fiskenaesset anorthositic complex, West Greenland: clues to late Archean mantle processes. In: Kusky, T.M., Zhai, M.G., Xiao, W. (Eds.), The Evolving Continents: Understanding Processes of Continental Growth, vol. 338. Geological Society, London, Special Publications, pp. 197–212.
Ruskov, T., Spirov, I., Georgieva, M., Yamamoto, S., Green, H.W., McCammon, C.A., Dobrzhinetskaya, L.F., 2010. Mossbauer spectroscopy studies of the valence state of iron in chromite from the Luobusa massif of Tibet: implications for a highly reduced deep mantle. J. Metamorph. Geol. 28, 551–560.
Saha, A., Santosh, M., Ganguly, S., Manikyamba, C., Ray, J., Dutta, J., 2018. Geochemical cycling during subduction initiation: evidence from serpentinized mantle wedge peridotite in the south Andaman ophiolite suite. Geosci. Front. 9, 1755–1775.
Saunders, J.E., Pearson, N.J., O'Reilly, S.Y., Griffin, W.L., 2015. Sulphide metasomatism and the mobility of gold in the lithospheric mantle. Chem. Geol. 410, 149–161.
Sinton, C.W., Duncan, R.A., Storey, M., Lewis, J., Estrada, J.J., 1998. An oceanic flood basalt province within the Caribbean plate. Earth Planet Sci. Lett. 155, 221–235.
Taylor, B., Martinez, F., 2003. Back-arc basin systematics. Earth Planet Sci. Lett. 210, 481–497.
Tokuyama, H., Batiza, R., 1981. Chemical composition of igneous rocks and origin of the sill and pillow-basalt complex of Nauru Basin, southwest Pacific. Initial Rep. D.S.D.P. 61, 673–687.
Torró, L., Proenza, J.A., Farré-de-Pablo, J., Colomer, J.M., García-Casco, A., Melgarejo, J.C., Alfonso, P., Gubern, A., Gallardo, E., Cazañas, X., Chávez, C., del Carpio, R., León, P., Espaillat, J., Lewis, J.F., 2016. Mineralogy, geochemistry and sulfur isotope characterization of Cerro de Maimón (Dominican Republic), San Fernando and Antonio (Cuba) Lower Cretaceous VMS deposits: formation during subduction initiation of the Proto-Caribbean lithosphere within a fore-arc. Ore Geol. Rev. 72, 794–817.

Torró, L., Proenza, J.A., Garcia-Casco, A., Farré-de-Pablo, J., del Carpio, R., León, P., Chávez, C., Domínguez, H., Brower, S., Espaillat, J., Nelson, C., Lewis, J.F., 2017. La geoquímica de la Formación Maimón (Cordillera central, República dominicana) revisada. Bol. Geol. Min. 128, 517–539 (in Spanish).

Uysal, I., Tarkian, M., Sadiklar, M.B., Zaccarini, F., Meisel, T., Garuti, G., Heidrich, S., 2009. Petrology of Al- and Cr-rich ophiolitic chromitites from Mugla, SW Turkey: implications from composition of chromite, solid inclusions of platinum-group mineral, silicate, and base-metal mineral, and Os-isotope geochemistry. Contrib. Mineral. Petrol. 158, 659–674.

Villanova-de-Benavent, C., Proenza, J.A., Galí, S., Garcia-Casco, A., Tauler, E., Lewis, J.F., Longo, F., 2014. Garnierites and garnierites: textures, mineralogy and geochemistry of garnierites in the Falcondo Ni-laterite deposit, Dominican Republic. Ore Geol. Rev. 58, 91–109.

Wilson, M., 1989. Igneous Petrogenesis. Unwin Hyman, London.

Wu, Y., Xu, M., Jin, Z., Fei, Y., Robinson, P.T., 2016. Experimental constraints on the formation of the Tibetan podiform chromitites. Lithos 245, 109–117.

Xiong, F., Yang, J., Robinson, P.T., Xu, X., Liu, Z., Li, Y., Li, J., Chen, S., 2015. Origin of podiform chromitite, a new model based on the Luobusa ophiolite, Tibet. Gondwana Res. 27, 525–542.

Xu, X., Yang, J., Robinson, P.T., Xiong, F., Ba, D., Guo, G., 2015. Origin of ultrahigh pressure and highly reduced minerals in podiform chromitites and associated mantle peridotites of the Luobusa ophiolite, Tibet. Gondwana Res. 27, 686–700.

Yamamoto, S., Komiya, T., Hirose, K., Maruyama, S., 2009. Coesite and clinopyroxene exsolution lamellae in chromites: in-situ ultrahigh-pressure evidence from podiform chromitites in the Luobusa ophiolite, Southern Tibet. Lithos 109, 314–322.

Yang, J.S., Meng, F., Xu, S., Robinson, P.T., Dilek, Y., Makeyev, A.B., Wirth, R., Wiedenbeck, M., Cliff, J., 2015. Diamonds, native elements and metal alloys from chromitite of the Ray-Iz ophiolite of the Polar Urals. Gondwana Res. 27, 459–485.

Zaccarini, F., Garuti, G., Proenza, J.A., Campos, L., Thalhammer, O.A.R., Aiglsperger, T., Lewis, J., 2011. Chromite and platinum-group-elements mineralization in the Santa Elena ophiolitic ultramafic nappe (Costa Rica): geodynamic implications. Geol. Acta 9, 407–423.

Zhang, Y., Song, S., Yang, L., Su, L., Niu, Y., Allen, M.B., Xu, X., 2017. Basalts and picrites from plume-type ophiolite in the South Qilian accretionary belt, Qilian orogen: accretion of a Cambrian oceanic plateau? Lithos 278–281, 97–110.

Zhou, M.F., Keays, R.R., Kerrich, R.W., 1998. Controls on platinum-group elemental distributions of podiform chromitites: a case study of high-Cr and high-Al chromitites from Chinese orogenic belt. Geochem. Cosmochim. Acta 62, 677–688.

Zhou, M.-F., Robinson, P., Bai, W.-J., 1994. Formation of podiform chromitites by melt/rock interaction in the upper mantle. Miner. Deposita 29, 98–101.

Zhou, M.F., Robinson, P.T., Malpas, J., Li, Z.J., 1996. Podiform chromites in the Luobusa Ophiolite (Southern Tibet): implications for melt–rock interaction and chromite segregation in the upper mantle. J. Petrol. 37, 3–21.

Zhou, M.F., Robinson, P.T., Malpas, J., Aitchison, J., Sun, M., Bai, W.J., Hu, X.F., Yang, J.-S., 2001. Melt/mantle interaction and melt evolution in the Sartohay high-Al chromite deposits of the Dalabute ophiolite (NW China). J. Asian Earth Sci. 19, 517–534.

Zhou, M.F., Robinson, P.T., Su, B.X., Gao, J.F., Li, J.W., Yang, J.S., Malpas, J., 2014. Compositions of chromite, associated minerals, and parental magmas of podiform chromite deposits: the role of slab contamination of asthenospheric melts in suprasubduction zone environments. Gondwana Res. 26, 262–283.